Article:

Pang, X., Wang, G., Mountney, N.P. orcid.org/0000-0002-8356-9889 et al. (6 more authors) (2023) Prediction of lamina structure and reservoir quality in shale using well logs: The Cretaceous Qingshankou Formation, Gulong Sag, Songliao Basin, China. Geoenergy Science and Engineering, 227. 211827. ISSN 2949-8929

https://doi.org/10.1016/j.geoen.2023.211827

Prediction of lamina structure and reservoir quality in shale using well logs: the Cretaceous Qingshankou Formation, Gulong Sag, Songliao Basin, China

Xiaojiao Pang[1,2], Guiwen Wang[1,2], Nigel P. Mountney[3], Lichun Kuang[1,2], Xin Zhao[1,2], Yidi Zhao[1,2], Hongbin Li[1,2], Zongyan Han[1,2], Han Tian[2]

1. State Key Laboratory of Petroleum Resources and Prospecting, China University of Petroleum (Beijing), Beijing 102249, China

2. College of Geosciences, China University of Petroleum (Beijing), Beijing, 102249, China

3. School of Earth and Environment, Institute of Applied Geophysics, University of Leeds, Woodhouse, Leeds, LS2 9JT

Corresponding author: Xiaojiao Pang, China University of Petroleum (Beijing), 18 Fuxue Road, Changping, Beijing China 102249. E-mail: xiaojiaopang0829@163.com

Prof. Guiwen Wang, China University of Petroleum (Beijing), 18 Fuxue Road, Changping, Beijing China 102249. Tel.: +861089733435; Fax.: +861089734158; E-mail: wanggw@cup.edu.cn

Abstract

Lamina structure is determined by composition, thickness, continuity, and mineral assemblage. Reservoir quality in oil shale reservoirs is determined by lamina structure, which controls hydrocarbon accumulation and migration. The prediction and evaluation of multi-scale lamina structures using geophysical well logs is challenging. Recent studies demonstrate that the lamina structure classification may be based on core observation and core analysis. However, there are no corresponding high-resolution geophysical logging methods to identify and categorize lamina structure continuously in a single well. Here, an experimental approach, involving an integrated analysis of cores, thin sections, well logs such as slabs and button conductivity curves of image logs (up to 5 mm vertical resolution), is used to characterize lamina structure. T_1-T_2 (T_1, longitudinal relaxation time, and T_2, transverse relaxation time) maps of nuclear magnetic resonance (NMR) logs is applied to clarify the relationships between the lamina structure, reservoir quality, and oil-bearing properties. Results demonstrate how lamina structure in shale can be divided into three types: laminated rocks, layered rocks, and massive rocks, according to observation of core at the lamina scale. The thickness of individual lamina is less than 0.01 m in the laminated rocks, and the layered rocks have bundles of genetically related laminae thickness ranging between 0.01 m—0.1 m. In massive rocks there is no visible layering. The well log response patterns of the three types of lamina structure are established so that the distribution of lamina structure can be predicted in a single well via well logs. Results show that the oil-bearing shale intervals are dominated by laminated rocks and layered rocks, accounting for 90% of the studied Qingshankou Formation. In addition, the layered rocks play an important role in improving reservoir quality and the laminated rocks present moderate reservoir quality. The massive rocks show poor reservoir quality. Moreover, an increased proportion of felsic mineral content favors increased oil potential in oil shale reservoirs. The method is generally applicable and is of value in developing predictive indicators of subsurface reservoir sweet spots in shale oil and gas exploration and development.

Key words: Shale oil; lamina structure; reservoir quality; image logs; T_1-T_2 map

1. Introduction

Recently, unconventional reservoirs have become a focus of exploration and development, (Zou et al., 2013; Newport et al., 2016; Soeder., 2017; Yang et al., 2019). Oil shale reservoirs are distributed worldwide. Examples from the USA include the Bakken shale in the Williston Basin (Saidian and Prasad., 2015), the Eagle Ford shale in southern Texas (Ko et al., 2017), and the Barnett shale in the Fort Worth Basin (Jarvie et al., 2007; Hill et al., 2007; Loucks et al., 2009). Examples from China include the Triassic Yanchang Formation in the Ordos Basin, the Cretaceous Qingshankou Formation in the Songliao Basin (Lin et al., 2021), the Jurassic Longmaxi Formation in Sichuan Basin (Tang et al., 2019), the Paleogene Kongdian Formation in the Bohai Bay Basin (Yang et al., 2019) and the Permian Lucaogou Formation in the Junggar Basin (Pang et al., 2022). The proportion of shale oil and gas has increased steadily since the “shale revolution”, indicating an important resource prospect in the future (Hou et al., 2021). In addition, established technologies – including horizontal well drilling, volume fracturing stimulation, and refracturing – make it possible to produce oil and gas from shales, in addition to from coarser-grain clastic sandstone reservoirs using conventional production techniques (Zou et al., 2017; Yang et al., 2019). However, the energy industry is facing technical challenges in terms of drilling, exploration, development, and production of unconventional resources. They are more difficult to extract because production typically requires fracturing the rock formation to allow resources to accumulate in sufficient quantities and flow from the well. The occurrence of laminae (bedding) and lamellation fractures determine reservoir quality and engineering quality in sales – described by paramters including, for example, brittleness index, in situ stress, and fracability. Laminae can change into bedding parallel fractures during burial, where subject to diagenesis and compaction. This may be helpful for oil and gas accumulation since it favors improved fracture network formation during the later fracturing (Lai et al., 2022a). It is important to investigate the controlling relationships of laminae and lamellation fractures upon reservoir quality and oil-bearing properties. Moreover, the characterization of multi-scale laminae can be obtained through a variety of observation methods and well log technologies; for example, the direct observation of cores, thin sections and scanning electron microscopy (SEM) photomicrographs, and the interpretation of conventional geophysical logs using long-established techniques (Weidlicha et al., 2004; Xavier and Fagel., 2005; Chen et al., 2017; Li et al., 2020; Wang et al., 2021). Decimeter- to meter-scale bundles of genetically related laminae have been characterized using well log tools, including gamma-ray logs, deep and low resistivity logs, three porosity logs (density, neutron, and sonic interval transit time logs), and image logs (Wang et al., 2021; Lai et al., 2022b). However, there are no comprehensive logging evaluation methods for lamina structure and the relevant reservoir quality and oil-bearing properties controlled by small-scale lamina structure in oil shale reservoirs.

As a contribution to the worldwide growth in production and exploration of unconventional oil and gas, oil shale reservoirs have been discovered in the Upper Cretaceous Qingshankou and Nenjiang formations of the Gulong Sag, Songliao Basin, China (Bechtel et al., 2012; Xu et al., 2015). The Cretaceous Qingshankou Formation shale contains notable shale oil resources. Over the past two decades, high-resolution studies of the potential for hydrocarbon generation, the reconstruction of paleoenvironmental changes, the organic geochemistry, mineralogy, lithology, and lithofacies have been undertaken (Zhou and Littke, 1999; Xu et al., 2015; Liu et al., 2019; Sun et al., 2021). The shale reservoir in the Qingshankou Formation is characterized by self-generation and self-containment in the lacustrine source rocks (Li et al., 2017; Cui et al., 2020; Lin et al., 2021). There has been no migration (including micron-nano migration) identified; the hydrocarbon generation has not commenced expulsion because the limit of capillary resistance pressure, viscosity force, and friction force have not yet been exceeded (Feng et al., 2020). The reservoir is highly heterogeneous and characterized by complex sedimentary characteristics (Li et al., 2019; Yang et al., 2019; Hou et al., 2021). Notably, the presence of abundant laminae and bedding-parallel fractures differentiate this formation from other shale reservoirs developed in lacustrine palaeo-depositional environments (Li et al., 2019). These features are considered to be the key factors controlling the potential production of shale oil (Drager et al., 2016; Liu et al., 2019; Lai et al., 2022a). Therefore, it is essential to determine the role of the lamina structure in controls reservoir properties.

The aim of this study is to classify shale lamina structure, establish a logging evaluation method of multi-scale lamina structure, and assess their impact on reservoir quality. The reservoir characteristics of mineral composition, laminae types, lamina structure, and porosity are described through the core photos, XRD, and porosity experiment. The multi-scale lamina structure is identified by advanced well-log analysis, especially using image logs (slabs and button conductivity curves). These techniques are used to identify the millimeter- to meter-scale bundles of genetically related laminae according to their high resolution (5 mm). This allows for the lamina structure to be determined in a single well. T_1-T_2 maps of single and stacked depth derived from 2D NMR logs are used to characterize the reservoir quality and oil-bearing properties. This study provides essential insights into the quality and oil-bearing properties of a shale reservoir. The results can provide guidance for shale oil and gas exploration and development more widely.

2. Geological setting

The Songliao Basin is a significant and petroliferous basin in northwestern China, which spans three provinces, including Heilongjiang, Jilin, Liaoning, and Inner Mongolia; it covers more than 287,000 km^2 (Ge et al., 2010; Li et al., 2021a). The basin is divided into six tectonic units: the southwestern slope zone, southwestern uplift zone, northern uplift zone, central depression zone, northeastern uplift zone, and southeastern uplift zone (Fig. 1) (Li et al., 2021; Lin et al., 2021). Different sedimentary facies accumulated in the different tectonic zones: for example, alluvial-fan and fan-delta successions are located adjacent to steep basin-margin slopes, whereas braided rivers deltas developed across gently inclined slopes (Ge et al., 2010). A semi-deep to the deep lake (lacustrine) succession was accumulated in the depression zones (Ge et al., 2010).

The Gulong Sag is located in the western central depression zone of the northern basin; it covers an area of 3,700 km^2 (Chen et al., 2013; Li et al., 2021). Early Cretaceous strata in Gulong Sag can be divided into four formations: Shahezi Formation, Yingcheng Formation, Denglouku Formation, and Quantou Formation, from the bottom to the top (Li et al., 2017; Feng et al., 2020; Li et al., 2021). Additionally, late Cretaceous strata consist of the Qingshankou Formation, Yaojia Formation, Nenjiang Formation, Sifangtai Formation, and Mingshui Formation from the bottom to the top (Li et al., 2017; Feng et al., 2020; Li et al., 2021). The Qingshankou Formation, which conformably overlies the Quantou Formation and conformably underlies the Yaojia Formation, has abundant hydrocarbon resources and great exploration and development potential in shale oil (Feng et al., 2020; Li et al., 2021).

The Qingshankou Formation is subdivided into two members. Member 1 of the Qingshankou Formation covers an area of 4,200 km^2; Member 2 covers an area of 2,800 km^2, and is deposited after Member 1 (Pang et al., 2021; Li et al., 2021). The main sedimentary facies of the Qingshankou Formation were semi-deep to deep lakes that were rich in organic matter. Member 1 accumulated during a development of a maximum flooding surface, contributing to shale oil and gas accumulation (Li et al., 2020). In addition, the formation of organic pores and bedding-parallel fractures attributed to the hydrocarbon generation evolution during the burial, and thermal history were also essential for oil and gas accumulation and generation (Li et al., 2020; Feng et al., 2020; Lai et al., 2021).

3. Data and methods

In our study, five key wells named Wells A, B, X, Y, and Z are selected to predict the oil shale reservoir quality of the Cretaceous Qingshankou Formation, Gulong Sag, Songliao Basin (Fig.1c). More than 1600 core photos taken from Well B and Well X were used to observe the characteristics of lithologies and lamina structure of the Qingshankou Formation. Optical microscopy and X-ray Diffraction (XRD) were used to complement mineral characterization, identify types of pore space and observe oil-bearing properties. A total of 297 core samples selected from Well X were prepared for XRD measurement using machine PANalytical X'Pert Powder. These samples are roughly crushed to obtain various mineral types and contents using a system containing an experimental machine and analytical software. Thin sections were prepared according to a standard procedure, including freeze-drying and impregnation (Brauer and Casanova, 2001). Twenty-one core samples selected from Well A were cut to a thickness of 30 μm. They were mounted on slides ready for investigation under a microscope with both non-polarized and polarized light. All tests were completed at the State Key Laboratory of Petroleum Resources and Prospecting, China University of Petroleum Beijing. Petrophysical parameters including total porosity and effective porosity were obtained to evaluate the reservoir quality. The total porosity may be defined as all the pore space containing fluids (water, oil or gas), whether or not they are mobile. There are various definitions of effective porosity. In our study, effective porosity is defined as the ratio of interconnected pore volume to total pore volume in rocks. Two-hundred-and-six samples in the Cretaceous Qingshankou Formation in Well B have been analyzed using a Helium Porosity Instrument AP-121-003-1.

Wire-line log suites, comprising gamma-ray, array induction resistivity, and three porosity logs (bulk density, neutron porosity, and sonic interval transit time) of all these five wells in figure 1 were used to detect the meter scale bedding. Conventional well logs can only identify decimeter- to meter-scale stratal packages.

Borehole images derived from Schlumberger's fullbore formation microimager (FMI) are another effective source for detailed geological interpretation; these can be used to provide a continuous image of the sub-surface geology, as seen in the borehole wall (Kumar et al., 2014; Bize et al., 2015; Lai et al., 2018). Slabs derived from the image logs exhibit the planar surfaces, such as bedding planes, fractures, faults, as straight lines, as seen in the core slabs rather than the sinusoids typically seen on the borehole images (Fig. 2). Image logs are especially useful and well-suited to the identification of the laminae, especially in oil shale reservoirs. Appropriate image-log tools offer a high spatial resolution (up to 5 mm). Image logs can recognize laminae and laminae bundles ranging from millimeter- to meter-scale. In our study, image logs of three key wells (Wells X, Y, and Z) are available. Actually, the slab is the pseudo image of the strata, which represents the electrical contrasts. The slab displays clearer bedding characteristics than either the static or the dynamic images. When establishing the plate of well log response of three types of lamina structure, core photos are used for log calibration. At present, the identification of lamina type is undertaken manually, because no available and precise automatic identification method has yet been established.

Conventional Nuclear Magnetic resonance (NMR) logs are commonly used to evaluate the reservoir quality, including porosity and permeability, because only T_2 signals can be probed. Two-Dimensional Nuclear Magnetic Resonance (2D NMR) logs are commonly used to test both the longitudinal relaxation time (T_1) and the transverse relaxation time (T_2) of fluid-saturated rocks (Li et al., 2018). Various parameters of physical properties can be derived from NMR logs, including porosity, permeability, saturation, etc. The T_2 spectra profile, containing the characterization of pore size distribution and fluid property, is profitable for evaluating reservoir quality. Two-dimensional NMR maps (T_1-T_2 maps) are obtained and these will be used to exhibit the fluid types. These types consist of kerogen ($T_2 < 1$ ms, $T_1/T_2 > 100$), absorbed oil (T_2 between 0.22 ms – 1 ms, T_1/T_2 between 25 – 100), free oil ($T_2 > 1$ ms, T_1/T_2 between 10 – 100), structural water ($T_2 < 0.22$ ms, $T_1/T_2 < 100$), absorbed water ($T_2 < 1$ ms, $T_1/T_2 < 10$), free water (T_2 1 ms — 10 ms, $T_1/T_2 < 10$), bulk oil and bulk water according to the response of each component in rocks (Li et al., 2018). The proton components can be effectively identified, and the pore fluid types and distributions in shales can be calculated according to the cut off values of T_2 and the ratio of T_1 to T_2 (Marc and Maria., 2016; Zhang et al., 2020). In addition, continuous T_1 and T_2 data allow independent fluid volume and distribution assessment, wettability comparisons, and quantification of asphaltene content. Collectively these observations provide general information for petrophysical models as an alternative to using conventional methods to evaluate oil and gas saturation (Zhang et al., 2020).

In this study, Combinable Magnetic Resonance logging (CMR-NG) was used to obtain continuous T_1 and T_2 spectra; T_1-T_2 maps were processed using Techlog 2019 Software. The logging data are measured by the new generation of high-resolution NMR logs with the shortest echo interval of 200 μs and a low resonance frequency of 2 MHz in the low magnetism field, which was developed by Schlumberger. Six groups of parameters were set. The wait times were 2s, 0.3s, 0.05s, 0.01s, 0.003s, and 0.0012s, respectively. The number of echoes were 1800, 600, 100, 50, 20, and 20. The repetition counts were 1, 2, 10, 30, 50 and 50. The Echo spacings were 0.2 ms, 0.2 ms, 0.2 ms, 0.2 ms, 0.28 ms and 0.28 ms. Two key wells (Well Y with a study-interval thickness of 136.8 m) and Well Z (137.9 m) were examined to study shale deposits of the Qingshankou Formation in terms of their reservoir quality and oil-bearing properties. The quality control (QC) process is shown in figure 3. A spectrum of T_1 and T_2 can be obtained every 190.5 mm (Fig. 4A); abundant nuclear magnetic resonance spectra data, therefore, are available to characterize the reservoir quality and oil-bearing property. The T_1 and T_2 spectra distribution and the T_1-T_2 maps of single or stacked depth were obtained after NMR logs processing through Software Techlog 2019 (Fig. 4B, 4C). Due to the lack of calibration of laboratory data for 2D NMR, the T_2 and T_1/T_2 cut-offs relating to different fluid types cannot be defined. Therefore, the oil-bearing property was qualitatively evaluated according to the energy cluster position displayed in T_1-T_2 maps. The T_2 spectra are used to help characterize the reservoir quality, and the T_1-T_2 maps provide insight into fluid properties (Xu et al., 2023).

4. Results

4.1. Petrology characteristics

Figure 5 shows the mineralogical compositions of the shales in the Qingshankou Formation of Gulong Sag. Insights through the XRD analysis, the dominant minerals consist of terrigenous clastics, carbonates, and clay minerals. The contents of quartz, feldspar, calcite, dolomite and clay mineral are 0.7—43.4%, 1.3—53.9%, 0—76.7%, 0—96.6%, and 0—79.0%, respectively. The average contents of quartz, clay minerals, feldspar, dolomite, calcite, pyrite, and siderite accounted for 30.7%, 29.6%, 21.3%, 8.9%, 5.6%, 3.6%, and 0.4%, respectively in order of decreasing abundance. The high proportion of clay minerals in the shale of the Gulong Sag distinguishes it from other types of shales. Intergranular pores develop between mineral grains and crystals, including quartz, feldspar, carbonates, and clay (Loucks et al., 2010). This pore type is profitable for the formation of high reservoir quality, followed by intraparticle pores. Additionally, intragranular pores can usually be detected in particles, including in feldspar and pyrite (Loucks et al., 2010; Milliken et al., 2013). Organic matter pores can be detected in organic matters with small diameters (Loucks et al., 2010; Kuila et al., 2014; King et al., 2015).

The dominant lithologies are shale, mudstone, siltstone, shell limestone, and dolostone (Fig. 6). Gray-black shales are characterized by multi-scale laminae (the laminae density). Gray-white siltstones observed with laminae in cores accounted for a bit proportion. Only 1 m thickness of siltstones are observed in Well Y among all these five key studied wells. Well Y. The siltstones are attributed to terrigenous clastic input during an episode of falling lake level (Liu et al., 2019; Lin et al., 2021). Dolostone and bioclastic limestone are present in gray-white colors in the cores, accounting for 16%. Moreover, palaeobiota and palaeoflora (shell, algae) are preserved in the limestone, which can be identified by hydrochloric acid.

The oil shale reservoir in the Qingshankou Formation of the Gulong Sag, Songliao Basin, has a high reservoir quality characterized by an effective porosity of 0.5—12.1%, with an average value of 7.0% (Fig. 7). The total porosity ranges from 1.2% to 14.4%, with an average value of 9.5% (Fig. 7). The "sweet spot", distributed in the first Member and the lower part of the second Member in the Qingshankou Formation, is characterized by a total porosity of 6.2%—11.6%, with an effective porosity of 2.3%—7.1% (Cui et al., 2020). The main reservoir space consists of a great abundance of nanopores and a small number of micropores. Microfractures improve the reservoir seepage capacity (Li et al., 2017).

4.2. Multi-scale lamina structure

4.2.1. Three types of lamina structure

The multi-scale lamina can be divided into three types, including laminated rocks (the thickness of the layer is less than 0.01 m), layered rocks (the bundles of genetically related laminae thickness ranging between 0.01 m—0.1 m), and massive rocks (no varve or layer spacing > 0.1 m) according to the core observation (Fig. 8). However, there are a few differences in various lithologies. All laminated rocks, layered rocks, and barely massive rocks can be observed in shales. Three types of laminae can be observed in siltstone, but only massive rocks appear in mudstone, limestone, and dolostone (Fig. 6). Furthermore, laminated rocks can be classified into bright lamina (carbonate lamina and felsic lamina) and dark lamina (organic lamina and clay mineral lamina) according to the mineral assemblage through the microscopic inspection in shale reservoirs (Fig. 6). The different bright and dark laminae consist of various lamina structures based on their superposition sequence, which indicates the sedimentary processing and environment (Dräger et al., 2016). Lamina records have been shown to provide reliable records of spring discharges and variability therein (Sander et al., 2002). Lamina structure records are preserved in fine-grained sedimentary rocks providing possibilities for high-resolution climatic and environmental reconstructions (Jokinen et al., 2015; Haltia et al., 2021).

4.2.2. Well log expressions of various lamina

In addition, there are many studies about the interpretation of the lamina record and information preserved in its layers (Haltia et al., 2021). However, the continuous expressions of lamina preserved in the reservoir (especially in shale oil and gas) remain scarce. A new method is proposed to continuously evaluate the lamina in a single well as the development of the new techniques. The slab and the button electrode curve derived from image logs with the highest resolution in well logging technologies are used to identify and classify the lamina types (Fig. 9, Table. 1). The dynamic slabs of image logs show the layer alternately exchange in color gradation (bright, orange, dark, and intermediate color) (Fig. 9). The button conductivity curve characterizes the layer in the form of both color gradation and amplitude variation of the curve (Fig. 9).

In laminated rocks, the thickness of a single layer is on a millimeter scale, indicating the laminae changes are less than 1 centimeter. A total of 59 layers can be observed in different colors within 0.5 meters (Fig. 9A). More than 84 amplitude variations (peaks and troughs) can be identified in 0.5 meters (Fig. 9A). It can be observed that the button conductivity curve shows serrated characterization (Fig. 9A).

The layered rocks show that the thickness of the individual layer is centimeter-scale, ranging from 1 centimeter to 10 centimeters, suggesting that the layers' changes are centimeter lamination. A total of 35 layers can be recognized on the slab, and almost 71 layers are observed on the button conductivity curve in 0.5 meters (Fig. 9B).

No layers in the massive rocks or the individual layer of massive rocks is greater than 10 centimeters. There are no layers that can be observed in 0.1-meter scale depth intervals in slab images, but thinner layers can be detected by the button conductivity curve (Fig. 9C). In addition, the button electrode curve exhibits a box-shaped feature (Fig. 9C). The mudstone and limestone/dolostone of massive rocks are characterized by the image logs or slabs with single dark and bright spots, respectively.

Shales were dominated by laminated rocks and layered rocks observed from core photos and characterized by FMI images especially slabs (Fig. 10A–10D). According to core observation, the interface between different laminae was flat and intermittent in shales (Fig. 10A–10D). The shales accounted for the most proportion of rocks in the Qingshankou Formation. Only massive rocks can be observed in mudstones, without obvious layers or laminae and the FMI images display a dark spot model (Fig. 10E). Three types of lamina structure can be detected in sandstones (Fig. 10F–10H). The boundary between various bedding is clear, and the interface was horizontal or wave and continuous (Fig. 10F–10H). From the core observation, laminated and layered rocks rarely appear in limestones and dolostones and the FMI images show a bright spot model (Fig. 10I). Via insight through the FMI image, the shale and mudstones are characterized by dark color in the static images (Fig. 10A—10E), whereas the static images display organic-yellow color in siltstones (Fig. 10F—10H). In addition, the FMI images show bright color pattern in limestones and dolostones (Fig. 10I). From the thin section observation, four types of laminae were identified, including clay lamina, felsic lamina, organic mineral lamina, and carbonate lamina (Fig. 10J).

4.2.3. T_1-T_2 maps obtained from NMR logs

Previous studies have established the classification scheme for grouping different hydrogen-bearing components in shales according to the NMR experiment (Kausik et al., 2016; Li et al., 2018; Mukhametdinova et al., 2021). These groups include kerogen, absorbed oil, free oil, structural water, absorbed water, free water, bulk oil and bulk water. However, NMR logging only responds to the formation of pore fluid without the effect of kerogen content. According to the T_2 and the ratio of T_1 to T_2 response of different fluid types, oil-bearing properties and mobility will be qualitatively and quantitatively characterized and evaluated. In this study, the oil-bearing property and reservoir quality were qualitatively evaluated by the location of energy clusters (hydrogen clusters). The energy cluster located in the upper-right corner of the T_1-T_2 map represents high reservoir quality and high oil saturation. On the contrary, the energy cluster located in the lower-left corner of the T_1-T_2 map indicates poor reservoir quality and low movable oil and water content (Fig. 11). Based on the lamina structure classification in the Cretaceous Qingshankou Formation in the Gulong Sag, Songliao Basin, three types of T_1-T_2 maps were identified in well Z.

Type I T_1-T_2 map of laminated rocks is characterized by two main energy clusters, the lower-left corner and the upper-right corner, representing different fluid types in various pore systems (Fig. 11A). The left corner energy cluster shows clay-bound water and bitumen in the intragranular pores and organic matter pores. The energy cluster in the right corner represents the movable water ($T_1 = T_2$, yellow-green parts) and movable oil ($T_1 > T_2$, red parts), indicating well oil-bearing property. Both the T_1 and T_2 distributions exhibit bimodal behaviors, implying the strong heterogeneous of laminated rocks. The short T_2 components represent the discontinuous pores of small sizes. The T_2 components larger than 30 ms correspond to the large pores (dissolution pores) and well connectivity pores and throats, resulting in the good reservoir quality (Lai et al., 2019).

Type II T_1-T_2 map corresponding to layered rocks shows three clusters, the lower-left corner, the upper right corner, and the part along the waterline ($T_1 = T_2$) (Fig. 11B). The left corner part is located lower than in laminated rocks and near the waterline due to more immovable water in small pores. The part alongside the waterline is characterized by movable water in connectivity pore space. The energy intensity of the upper right corner is lower than in laminated rocks, which displays in green color rather than red.

The energy cluster of type III representing massive rocks, the T_1-T_2 map, is concentrated in the lower-left corner (short T_1 and T_2 components), representing bitumen, clay bound water, and oil in organic porosity (Fig. 11C). The T_2 spectrum shows unimodal behavior. The T_2 relaxation time is restricted to within a narrow range (< 30 ms), indicating more pores of small sizes lacking large pores. Obviously, this type of rock corresponds with poor reservoir quality.

5. Discussion

5.1. Lamina distribution prediction via well logs

The dominant laminae structure is layered rocks, followed by laminated rocks, with only a small number of instances of massive rocks identified in the Cretaceous Qingshankou Formation in Well X (Fig. 12). In total, 1,178 layers are identified in the 482.5 m thickness Qingshankou Formation of Well X. 482 layers of laminated rocks account for 45% thickness, and the thickness of a single layer ranges from 0.04 m to 2.92 m with an average value of 0.45 m. The layered rocks, with the maximum proportion of 50.4% thickness in these three types, comprise 563 layers, and the average thickness of each layer is 0.43 m ranging from 0.02 m to 5.23 m. Only 4.6% of the massive rocks are recognized, containing 133 layers.

In contrast, laminated rocks account for the largest proportion in Well Y. In total, 453 layers are identified in the 136.8 m thickness in the Qingshankou Formation (Q1-Q9). In total, 198 layers of laminated rocks with 80.08 m thickness are recognized, and single layers range in thickness from 0.07 m to 20.2 m, with an average of 0.4 m. There are 183 layers of layered rocks with 47.57 m thickness, and the average thickness of every single layer is 0.26 m (the minimum of 0.04 m and the maximum of 0.95 m). Only 72 layers of massive rocks can be classified in Well Y, and their total cumulative thickness is 9.15 m.

From the distribution prediction via well logs above, it can be concluded that laminated rocks and layered rocks are the main laminae structure in the Cretaceous Qingshankou Formation in Gulong Sag Songliao Basin. The laminae development makes it unique from other types of shale worldwide, for example the Barnett Shale in the Fort Worth Basin in the United States, the Permian Lucaogou Formation in Jimusar Sag in Junggar Basin in China , and the Triassic Yanchang Formation in the Ordos Basin in China (Loucks et al., 2009; Xi et al., 2015, 2020; Zou et al., 2019).

There is a specific correspondence between the conventional well logs and the lamina structure (Wang et al., 2021). The massive rocks contain high carbonate content, corresponding to high resistivity and low gamma values (Fig. 12). Conversely, the laminated rocks are characterized by high gamma value attributed to the high content of clay minerals. The layered rocks contain more felsic resulting in medium resistivity and gamma value. The main controlling factors of various lamina types are complex, including climate change, lake level fluctuation, and the injection of terrigenous detritus (Fagel et al., 2021). In addition, it can be observed from Fig. 12 that the resolution of the conventional well logs is low, and the curves change gently. Therefore, it is challenging to identify the lamina structure through the conventional well logs. However, the high-resolution image logs (5 mm) are profitable for evaluating lamina structure, especially the slabs and button conductivity curve derived from the image logs.

5.2. Prediction of lamina structure as a control on reservoir quality and oil content

T_1-T_2 maps obtained from the NMR logs can be used to describe the fluid types, oil-bearing, and porous systems (Guo et al., 2020; Ge et al., 2022; Pang et al., 2022). In our study, the T_1-T_2 maps are divided into three types corresponding to three types of lamina structure.

Figure 13 shows the lamina structure distribution and corresponding T_1 and T_2 spectra of the Cretaceous Qingshankou Formation in Well Y. The interpretation interval A is typical layered rocks. The T_1-T_2 map is characterized by two energy clusters, the left corner in red color, a little away from the center, representing less immovable fluid (Fig. 13A). The upper right corner in green color implies less movable fluid than the right corner in red color (Fig. 13A). Consequently, the T_1-T_2 map of interval A shows higher reservoir quality and better oil-bearing properties. The massive rocks mainly correspond with intervals with short T_2 components, and the T_1-T_2 map shows only one energy cluster in the lower left (Fig. 13B). Interval C, the same as interval A, is representative layered rocks (Fig. 13C). The laminated rocks are related to the intervals with long T_2 distribution and high amplitudes but lower than layered rocks. In addition, two energy clusters can be observed in the T_1-T_2 map, and the upper right corner cluster is in green, indicating the good reservoir quality and oil-bearing potential (Fig. 13D).

Interpretation interval A is a representative layered rock, and the T_2 spectra exhibit a long T_2 relaxation time with high amplitude (Fig. 14A). Two energy clusters can be observed in the T_1-T_2 map indicating the good reservoir quality and oil mobility (Fig. 14A). The interval B is a typical laminated rock (Fig. 14B). The T_2 spectra show a long T_2 relaxation time but lower amplitude in the long T_2 components (Fig. 14B). There are two energy clusters in the T_1-T_2 map, but the energy is weak in the upper right corner implying less oil mobility (Fig. 14B). Therefore, from investigating the relationships between lamina structure and NMR logs (T_2 distribution and T_1-T_2 maps), the layered rocks have the best reservoir quality and most favorable oil-bearing properties in the shales, followed by laminated rocks.

Additionally, the oil test can approve these conclusions that the more layered rocks develop, the better reservoir quality and oil yield productivity are (Fig. 14C, 14D). The oil test results show that Well Z is more productive than Well Y (Fig. 14C, 14D). The laminated rocks account for 42.1%, and the layered rocks is 49.9% in the Qingshankou Formation (strata Q3 to Q4) in well Z (Fig. 14C). However, the laminated rock's proportions are up to 67.1%, and the layered rocks account for 27.9% in well Y (strata Q3 to Q4) (Fig. 14D).

The lamina structure and oil-bearing properties are interpreted in Well Z (Fig. 15). Interpretation intervals A and D are typical laminated rocks, which show different T_1-T_2 maps. Interval A exhibits better reservoir quality and oil potential than interval B, attributed to the less clay mineral content (Fig. 15). The intervals B and C are representative layered rocks, whereas the reservoir quality of interval C is better than interval B since there are fewer clay minerals (Fig. 15). Therefore, from investigating the relationships between lamina structure, mineral composition, and T_1-T_2 maps, the reservoir quality and oil-bearing properties increase with decreasing clay mineral content in shales in different lamina structures.

In addition, oil is mainly distributed in the interface between mudstone and sandstone or carbonate, but less in carbonate or sandy layers (Shao et al., 2021). Light components of high mature oil are relatively accumulated in carbonate or felsic laminae, while heavy components are relatively enriched in clay or organic matter laminae (Shao et al., 2021; Zhang et al., 2021).

However, the controlling factors of reservoir quality are complicated. The layered rocks combined with high content of organic matter, favorable lithofacies, and fractures (including parallel fractures) may lead to a high-quality reservoir and oil mobility.

6. Conclusions

This study elucidates the relationship between lamina structure, reservoir quality, and oil potential in shale, taking the Cretaceous Qingshankou Formation in Gulong Sag, Songliao Basin, as an example.

The main mineralogical compositions of the shales in the Qingshankou Formation are quartz, feldspar, clay minerals, and a small number of carbonates. According to the core observation in oil shale, the lamina structure is classified into three types: laminated rocks, layered rocks, and massive rocks. Both laminated rocks and layered rocks can be observed in shales, but on rarely massive rocks can be observed. Three types of laminae can be observed in siltstone, but only massive rocks appear in mudstone, limestone, and dolostone. The image logs, slabs, and button conductivity curves are efficient ways to predict a single well's lamina distribution. The Qingshankou Formation is dominated by laminated rocks and layered rocks, which account for more than 90 percent. According to the energy clusters, the T_1-T_2 maps are classified into three types: type I, II, and III, which correspond to laminated rocks, layered rocks and massive rocks, respectively. Among all the lamina structures, layered rocks show a good reservoir quality and high oil accumulation, followed by laminated rocks. In contrast, massive rocks present a poor reservoir quality without oil production. The greater the clay mineral content, the poorer the quality and oil potential of the shale reservoirs.

Acknowledgments

This work was supported by the PetroChina Research Institute of Petroleum Exploration and Development and PetroChina Daqing Oilfield Company. We would like to give our sincere gratitude to them for providing samples and data access. The authors would also like to thank the National Natural Science Foundation of China (Grant No. 42002133, 42072150) for the financial support and permission to publish this paper. We sincerely appreciate the American Association of Petroleum Geologists Foundation and the Southeast Asia Petroleum Exploration Society Grant. We appreciate the editorial staff and all four reviewers for their diligent work with enthusiasm and patience.

References

Bechtel, A., J. Jia, S. A. I. Strobl, R. F. Sachsenhofer, Z. Liu, R. Gratzer, and W. Pu¨ ttmann, 2012, Palaeoenvironmental conditions during deposition of the Upper Cretaceous oil shale sequences in the Songliao Basin (NE China): Implications from geochemical analysis. Organic Geochemistry, 46, 76–95.

Bize E., Karoon A T., Laronga R., Bize-Forest N. 2015. Virtual Core: State-of-the-Art Wireline Technologies To Provide a Viable Substitute for Whole Conventional Coring. Offshore Technology Conference.

Brauer A and Casanova J. 2001. Chronology and depositional processes of the laminated sediment record from Lac d'Annecy, French Alps. Journal of Paleolimnology 25(2): 163–177.

Chen F W., Lu S F., Huang Z K., Wang W W., Xie Z., Xiao H. 2013. Sedimentary characteristics and favorable exploration zone of K1qn1 in Gulong Depression of Songliao Basin. Journal of Central South University (Science and Technology), 44, 5, 1955－1963.

Chen, S.Y., Zhang, S., Liu, H.M., Yan, J.H. 2017. Discussion on mixing of fine-grained sediments in lacustrine deep water. Journal of Paleogeography, 19(2), 271–283.

Cui Baowen., Chen Chunrui., Lin Xudong., Zhao Ying., Cheng Xinyang., Zhang Yupeng., Lu Guoqiang. 2020. Characteristics and distribution of sweet spots in Gulong shale oil reservoirs of Songliao Basin. Petroleum Geology ＆ Oilfield Development in Daqing, 39, 3, 45–55.

Dräger Nadine., Theuerkauf Martin., Szeroczyńska Krystyna., Wulf Sabine., Tjallingii Rik., Plessen Birgit., Kienel Ulrike., Brauer Achim. 2016. Varve microfacies and varve preservation record of climate change and human impact for the last 6000 years at Lake Tiefer See (NE Germany). Research Paper, The Holocene, 1－15.

Fagel N., Pedreros P., Alvarez D., Tylmann W., Namur O., Da Silva A C., Jana P., Araneda A., Billy I., Schmidt S., Urrutia R. 2021. Last millennium climate variability of the varved Lake Jeinimeni geochemical record from NE Chilean Patagonia. Quaternary Science Reviews, 269, 107134.

Feng Z H., Liu B., Shao H M., Wang C., Hong S X., Wang J P., Pan H F., Wang Y C., Zhang A D., Tian S S., Chi Y A. 2020. The diagenesis evolution and accumulating performance of the mud shale in Qingshankou Formation in Gulong area，Songliao Basin. Petroleum Geology ＆ Oilfield Development in Daqing, 39, 3, 72–85.

GE Rongfeng., ZHANG Qinglong., WANG Liangshu., XIE Guo'ai., XU Shiyin., CHEN Juan., WANG Xiyong. 2010. Tectonic Evolution of Songliao Basin and the Prominent Tectonic Regime Transition in Eastern China. Geological Review, 56, 2, 180–193.

Ge Xinmin, Zhang Renxia, Liu Jianyu, Fan Yiren, Zhao Jier, Li Chaoliu, Hu Falong. 2022. NMR transverse relaxation of the clay-rich shale in inhomogeneous magnetic field: A numerical study. Computers & Geosciences, 166, 105174.

Guo J F., Xie R H., Xiao L Z. 2020. Pore-fluid characterizations and microscopic mechanisms of sedimentary rocks with three-dimensional NMR: Tight sandstone as an example. Journal of Natural Gas Science and Engineering, 80,103392.

Haltia E., Leppanen A P., Kallio A., Saarinen T. 2021. Sediment profile dating and reconstructing nuclear events from annually laminated lake sediments in northern Finland. Journal of Environmental Radioactivity, 233, 106611.

Hill, R.J., Zhang, E., Katz, B.J., et al. Modeling of gas generation from the Barnett shale, fort Worth basin, Texas. AAPG Bulletin, 2007, 91, 4, 501–521.

Hou Lianhua., Zou Caineng., Yu Zhichao., Luo Xia., Wu Songtao., Zhao Zhongying., Lin Senhu., Yang Zhi., Zhang Lijun., Wen Dingwei., Cui Jingwei. 2021. Quantitative assessment of the sweet spot in marine shale oil and gas based on geology, engineering, and economics: A case study from the Eagle Ford Shale, USA. Energy Strategy Reviews, 38, 100713.

Jarvie, D.M., Hill, R.J., Ruble, T.E. Unconventional shale-gas systems: the Mississippian Barnett Shale of north-central Texas as one model for thermogenic shale-gas assessment. AAPG Bulletin 2007, 91, 475–499.

Jokinen A., Sami, Virtasalo J., Joonas, Kotilainen T., Aarno, Saarinen, Timo, 2015. Varve microfabric record of seasonal sedimentation and bottom flow-modulated mud deposition in the coastal northern Baltic Sea. Marine Geology, 366, 79–96.

Kausik, R., Fellah, K., Rylander, E., Singer, P.M., Lewis, R.E., Sinclair, S.M., 2016. NMR relaxometry in shale and implications for logging. Petrophysics 57, 339–350.

King Jr HE, Eberle AP, Walters CC, Kliewer CE, Ertas D, Huynh C. 2015. Pore architecture and connectivity in gas shale. Energy & Fuels, 29, 1375–1390.

Ko, L.T., Loucks, R.G., Ruppel, S.C., et al. Origin and characterization of Eagle Ford pore networks in the south Texas Upper Cretaceous shelf. AAPG Bulletin 2017,101 (3), 387–418.

Kuila U, McCarty DK, Derkowski A, Fischer TB, Top´or T, Prasad M. 2014. Nano-scale texture and porosity of organic matter and clay minerals in organic-rich mudrocks. Fuel, 135, 359–73.

Kumar A., Laronga R., Kherroubi J., Bringer F., Kear G., Herrera J. 2014. Visualizing Borehole Images in a Slabbed-Core Format. EAGE, Borehole Geology Workshop, 12－15.

Lai Jin., Liu Bingchang., Li Hongbin., Pang Xiaojiao., Liu Shichen., Bao Meng., Wang Guiwen. 2022a. Bedding parallel fractures in fine-grained sedimentary rocks: recognition, formation mechanisms, and prediction using well log. Petroleum Science, https://doi.org/10.1016/j.petsci.2021.10.017

Lai J., Pang X., Xu F., Wang G., Fan X., Xie W., Chen J., Qin Z., Zhou Z. 2019. Origin and formation mechanisms of low oil saturation reservoirs in Nanpu Sag, Bohai Bay Basin, China. Marine and Petroleum Geology 110, 317–334.

Lai J., Wang G., Fan Q., et al. 2022b. Geophysical Well-Log Evaluation in the Era of Unconventional Hydrocarbon Resources: A Review on Current Status and Prospects. Surveys in Geophysics, 43:913–957

Lai J., Wang G., Wang S., Cao J., Li M., Pang X., Han C., Fan X., Yang L., He Z., Qin, Z. 2018. A review on the applications of image logs in structural analysis and sedimentary characterization. Marine and Petroleum Geology, 95, 139–166.

Li Canxing., Liu Dongdong., Xiao Lei., Jiang Zhenxue., Li Zhuo., Guo Jing. 2021a. Research into pore evolution in Cretaceous continental shales in the Songliao Basin. Petroleum Science Bulletin, 2, 181–195.

Li F., Zhao W Y., Guo A J., Chang T Y. 2021b. Quantitative characterization of rock pore structure and its computer application: a case study of Qingshankou Formation in Songliao Basin. Coal Engineering, 53, 7, 119－122.

Li J., Wang M., Lu S., Chen G., Tian W., Jiang C., Li Z. 2020. A new method for predicting sweet spots of shale oil using conventional well logs. Marine and Petroleum Geology, 113, 104097.

Li Jinbu., Huang Wenbiao., Lu Shuangfang., Wang Min., Chen Guohui., Tian Weichao., Guo Zhiqiang. 2018. Nuclear Magnetic Resonance T_1-T_2 Map Division Method for Hydrogen-Bearing Components in Continental Shale. Energy&Fuel, 32, 9043－9054.

Li Maowen., Ma Xiaoxiao., Jiang Qigui., Li Zhiming., Pang Xiongqi., Zhang Caitong. 2019. Enlightenment from formation conditions and enrichment characteristics of marine shale oil in North America. Petroleum Geology and Recovery Efficiency, 26, 1, 13–28.

Li S C., Zhang J Y., Gong F H., Zhu H., Bai Y F. 2017. The characteristics of mudstones of Upper Cretaceous Qingshankou Formation and favorable area optimization of shale oil in the north of Songliao Basin. Geological Bulletin of China, 36, 4, 654－663.

Lin Y F., Bai Y F., Zhao Y., Cheng X Y., Lv J C., Liu Z. 2021. Cyclic stratigraphy of fine-grained sedimentary rocks and sedimentary filling response characteristics of Member Qing-1 in Gulong Sag，Songliao Basin. Petroleum Geology ＆ Oilfield Development in Daqing, 40, 5, 29－39.

Liu B., Wang H L., Fu X F., Bai Y F., Bai L H., Jia M C., He B. 2019. Lithofacies and depositional setting of a highly prospective lacustrine shale oil succession from the Upper Cretaceous Qingshankou Formation in the Gulong sag, northern Songliao Basin, northeast China. AAPG Bulletin, 103, 2, 405－432.

Loucks, R. G., Reed, R. M., Ruppel, S. C., and Hammes, U. 2010, Preliminary classification of matrix pores in mudrocks: Gulf Coast Association of Geological Societies Transactions, 60, 435–441.

Loucks, R. G., Reed, R. M., Ruppel, S. C., Jarvie, D. M., 2009. Morphology, genesis, and distribution of nanometer-scale pores in siliceous mudstones of the Mississippian Barnett shale. Journal of Sedimentary Reservoir, 79, 848–861.

Marc Fleury., MariaRomero-Sarmiento. 2016. Characterization of shales using T1–T2 NMR maps. Journal of Petroleum Science and Engineering, 137, 55－62.

Milliken KL, Rudnicki M, Awwiller DN, Zhang T. 2013. Organic matter–hosted pore system, Marcellus formation (Devonian). Pennsylvania, AAPG Bulletin, 97, 177–200.

Mukhametdinova Aliya., Iwona Habina-Skrzyniarz., Andrey Kazak., Artur Krzyzak. 2021. NMR relaxometry interpretation of source rock liquid saturation — A holistic approach. Marine and Petroleum Geology, 132, 105165.

Newport, L. P., A. C. Aplin, J. G. Gluyas, H. C. Greenwell, and D. R. Gr¨ ocke, 2016. Geochemical and lithological controls on a potential shale reservoir: Carboniferous Holywell Shale, Wales: Marine and Petroleum Geology, 71, 198–210.

Pang Xiaojiao., Wang Guiwen., Kuang Lichun., Li Hongbin., Zhao Yidi., Li Dong., Zhao Xin., Wu Songtao., Feng Zhou., Lai Jin. 2022. Marine and Petroleum Geology, 137, 105492.

Pang Y M., Zhang Y Q., Cai M., Zhang H L., Guo Z Q. 2021. Technical and economic limit of horizontal well development for Gulong shale oil in Songliao Basin. Petroleum Geology & Oilfield Development in Daqing, 40, 5, 134－143.

Saidian, M., & Prasad, M. 2015. Effect of mineralogy on nuclear magnetic resonance surface relaxivity: A case study of Middle Bakken and Three Forks formations. Fuel, 161, 197-206.

Sander, M., Bengtsson, L., Holmquist, B., Wohlfarth, B., Cato, I., 2002. The relationship between annual varve thickness and maximum annual discharge. Journal of Hydrology, 263, 23–35.

Shao Hongmei., Gao Bo., Hong Shuxin., Li Lingling., Wang Jiping., Wang Yongchao., Bai Xuejing., Tan Wenli. 2021. Progress and application of the experimental technologies for the shale oil reservoirs: A case study on Gulong area in Songliao Basin. Petroleum Geology & Oilfield Development in Daqing, 39, 3, 97–106.

Soeder. D.J. 2017. The successful development of gas and oil resources from shales in North America, Journal of Petroleum Science and Engineering, 163, 399-420.

Sun Longde., Liu He, He Wenyuan., Li Guoxin., Zhang Shuichang., Zhu Rukai., Jin Xu., Meng Siwei., Jiang Hang. 2021. An analysis of major scientific problems and research paths of Gulong shale oil in Daqing Oilfield, NE China. Petroleum Exploration and Development. 48, 3, 527–540.

Tang Xianglu., Jiang Shu., Jiang Zhenxue., Li Zhuo., He Zhiliang., Long Shengxiang., Zhu Deyu. 2019. Heterogeneity of Paleozoic Wufeng-Longmaxi formation shale and its effects on the shale gas accumulation in the Upper Yangtze Region, China. Fuel, 239, 387–402.

Wang Song., Wang Guiwen., Huang Liliang., Song Lianteng., Zhang Yilin., Li Dong., Huang Yuyue. 2021. Logging evaluation of lamina structure and reservoir quality in shale oil reservoir of Fengcheng Formation in Mahu Sag, China. Marine and Petroleum Geology, 133, 105299.

Weidlicha O., Berneckerb M. 2004. Quantification of depositional changes and paleo-seismic activities from laminated sediments using outcrop data. Sedimentary Geology, 166, 11－20.

Xavier Boe¨s., Nathalie Fagel. 2005. Impregnation method for detecting annual laminations in sediment cores: An overview. Sedimentary Geology, 179, 185－194.

Xi, K.L., Cao, Y.C., Zhu, R.K., Shao, Y., Xue, X.J., Wang, X.J., Gao, Y., Zhang, J., 2015. Rock types and characteristics of tight oil reservoir in permian Lucaogou Formation, Jimsar sag. Acta Pet. Sin. 36, 1495–1507 (in Chinese with English abstract).

XI Kelai., LI Ke., CAO Yingchang., LIN Miruo., NIU Xiaobing., ZHU Rukai.,WEI Xinzhuo., YOU Yuan., LIANG Xiaowei., FENG Shengbin. 2020. Laminae combination and shale oil enrichment patterns of Chang 73 sub-member organic-rich shales in the Triassic Yanchang Formation, Ordos Basin, NW China. Petroleum Exploration and Development, 47, 6, 1244–1255.

Xu Chenyu, Xie Ranhong, Guo Jiangfeng, Jin Guowen, Fan Wenshuai, Xiao Lizhi. 2023, Comprehensive characterization of petrophysical properties in shale by solvent extraction experiments and 2D NMR. Fuel, 335, 127070.

Xu, J., A. Bechtel, R. F. Sachsenhofer, Z. Liu, R. Gratzer, Q. Meng, and Y. Song, 2015, High resolution geochemical analysis of organic matter accumulation in the Qingshankou Formation, Upper Cretaceous, Songliao Basin (NE China): International Journal of Coal Geology, 141–142, 23–32.

Yang Zhi., Zou Caineng., Wu Songtao., Lin Senhu., Pan Songqi., Niu Xiaobing., Men Guangtian., Tang Zhenxing., Li Guohui., Zhao Jiahong., Jia Xiyu. 2019. Formation, distribution and resource potential of the "sweet areas (sections)" of continental shale oil in China. Marine and Petroleum Geology, 102, 48–60.

Zhang Anda., Wang Jiping., Wang Yongchao., Hong Shuxin., Tan Wenli. 2021. Reservoir space types and oil occurrence of Gulong shale in Songliao Basin. Petroleum Geology & Oilfield Development in Daqing, 40, 5, 68–77.

Zhang Pengfei., Lu Shuangfang., Li Junqian., Chang Xiangchun. 2020. 1D and 2D Nuclear magnetic resonance (NMR) relaxation behaviors of protons in clay, kerogen and oil-bearing shale rocks. Marine and Petroleum Geology, 114, 104210.

Zhou, Y., and R. Littke, 1999, Numerical simulation of the thermal maturation, oil generation and migration in the Songliao Basin, Northeastern China. Marine and Petroleum Geology, 16, 8, 771–792.

Zou Caineng., Ding Yunhong., Lu Yongjun., Liu Xiangui., Chen Jianjun., Wang Xin., Yang Zhengming., Cai Bo., Yang Zhi., He Chunming., Wang Zhen., Luo Yutian.2017. Concept, technology and practice of “man-made reservoirs” development. Petroleum Exploration and Development,44, 1, 144–154.

Zou Caineng., Yang Zhi., Cui Jingwei., Zhu Rukai., Hou Lianhua., Tao Shizhen., Yuan Xuanjun., Wu Songtao., Lin Senhu., Wang Lan., Bai Bin., Yao Tingli. 2013. Formation mechanism, geological characteristics and development strategy of nonmarine shale oil in China. Petroleum Exploration and Development, 40, 1, 14–26.

Zou, C.N., Zhu, R.K., Chen, Z.Q., Ogg, J.G., Wu, S.T., Dong, D.Z., Qiu, Z., Wang, Y.M., Wang, L., Lin, S.H., Cui, J.W., Su, L., Yang, Z. 2019. Organic-matter-rich shales of China. Earth Science Review, 189, 51–78.

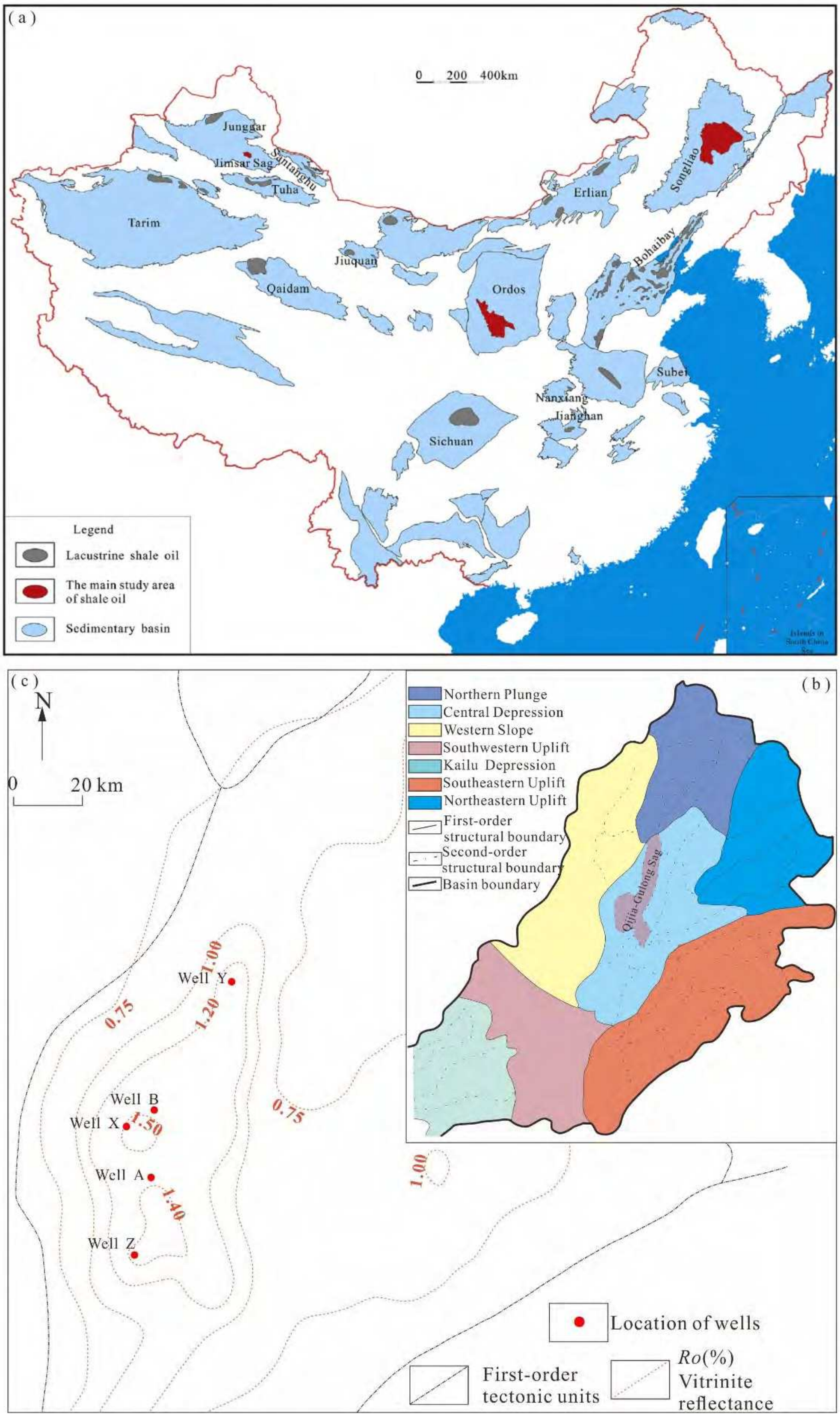

Figure 1. Location and geological map of Gulong Sag in Songliao Basin: (a) the Songliao Basin in China; (b) the location of Gulong Sag in Songliao Basin; (c) the location of the examined wells (Modified from Yang et al., 2019; Li et al., 2021).

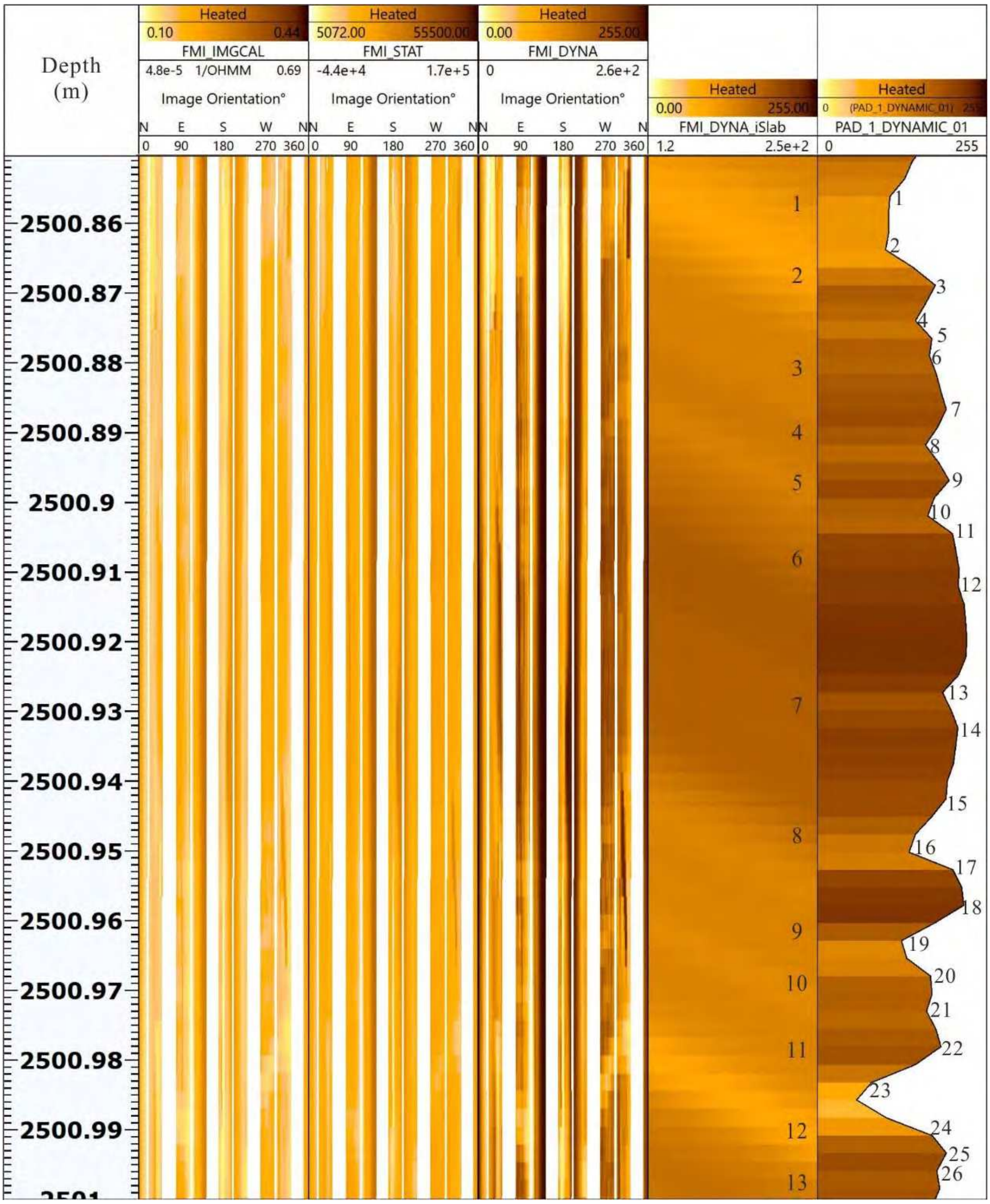

Figure 2. Slab image and button electrode curve derived from image logs of shale in the Cretaceous Qingshankou Formation, Gulong Sag, Songliao Basin (Well X). The first track is depth. The second track shows the full image log. The third track shows the static image log. The fourth track shows the corresponding dynamic image log. The fifth track displays the slab. The sixth track displays the button conductivity curve.

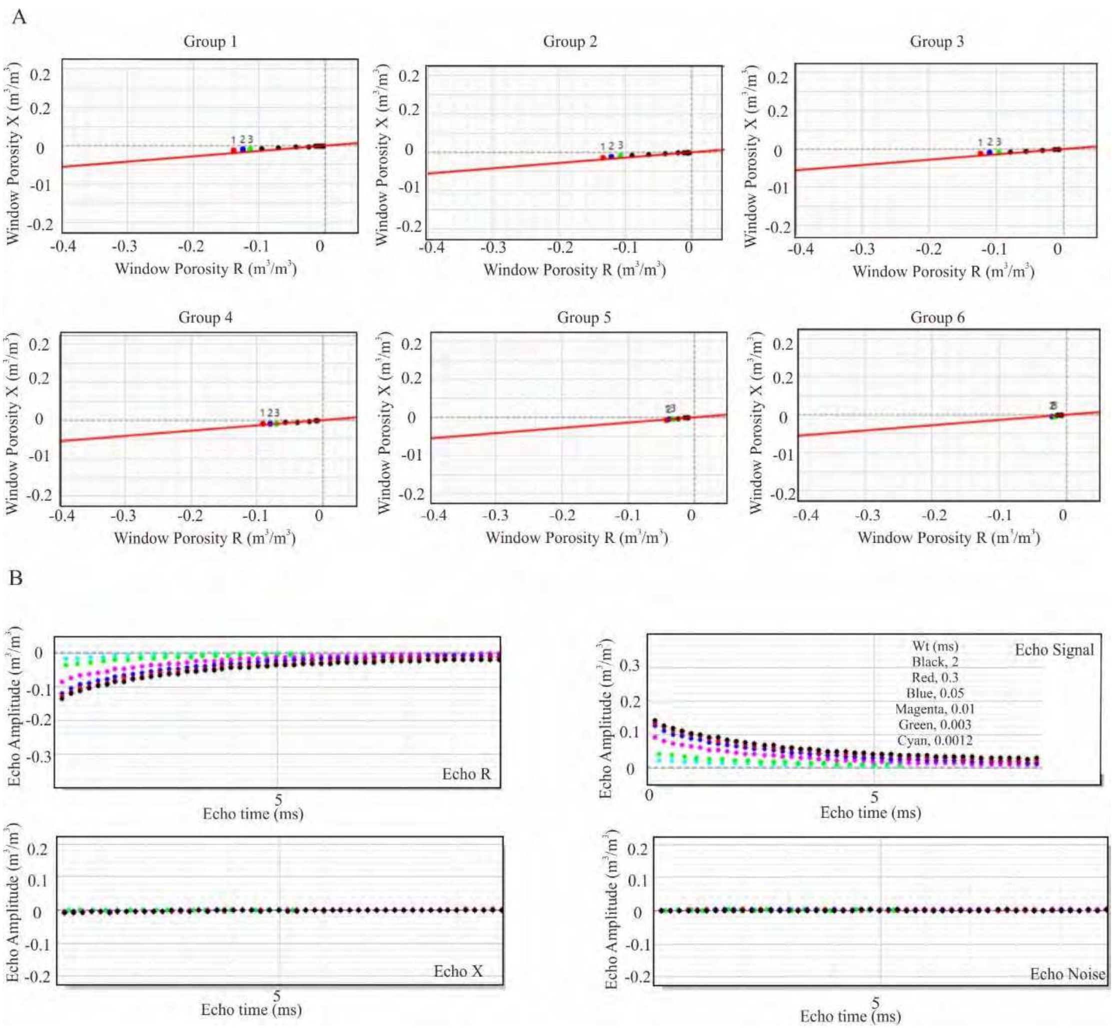

Figure 3. Reservoir quality control flag (Well Z), including Single phase quality control plot (A) and Echo quality control plot (B).

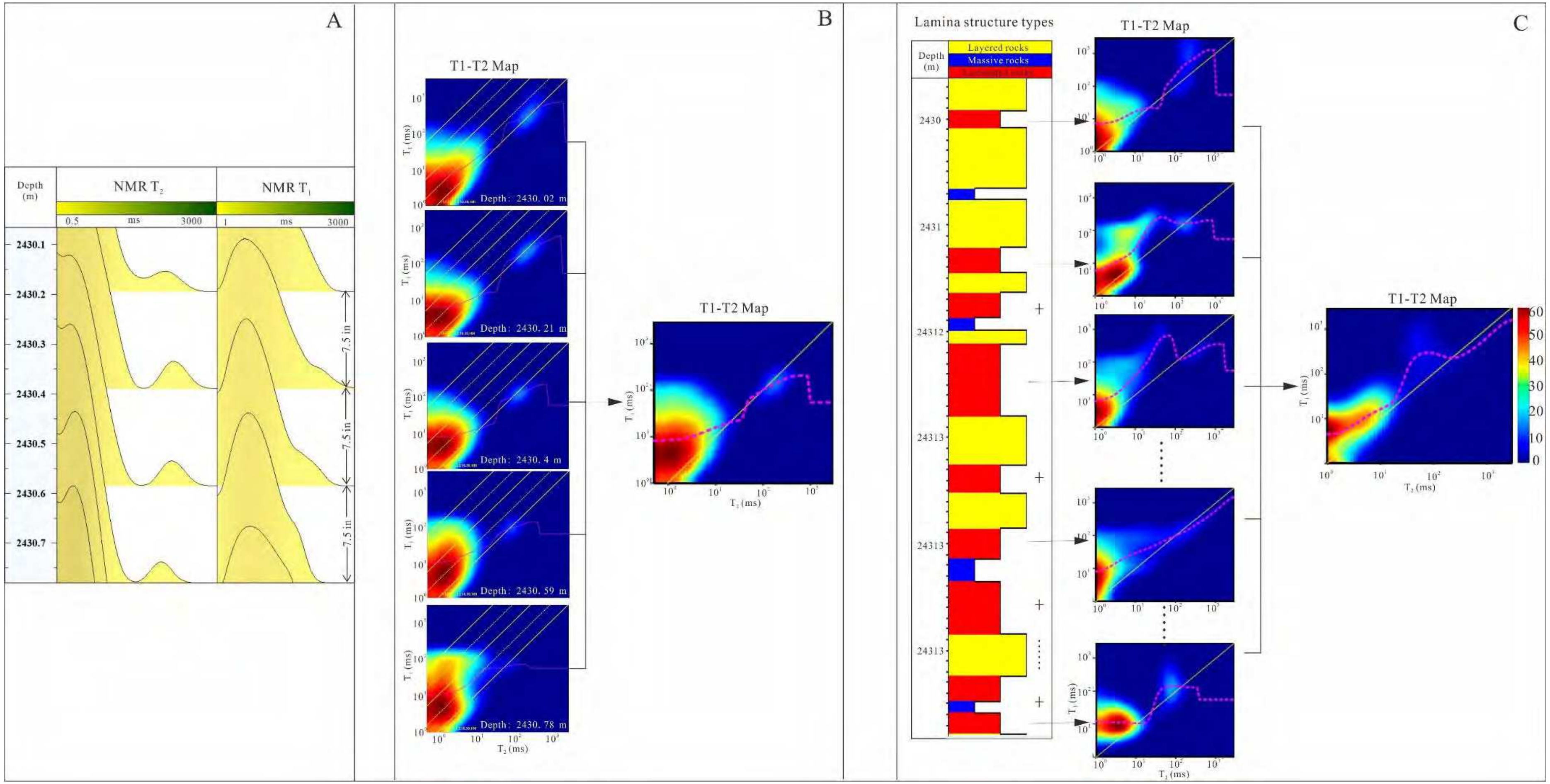

Figure 4. NMR T_1 and T_2 spectra (A), flowchart of T_1-T_2 maps of stacked depth (B), and flowchart of T_1-T_2 maps of stacked depth according to classification (C).

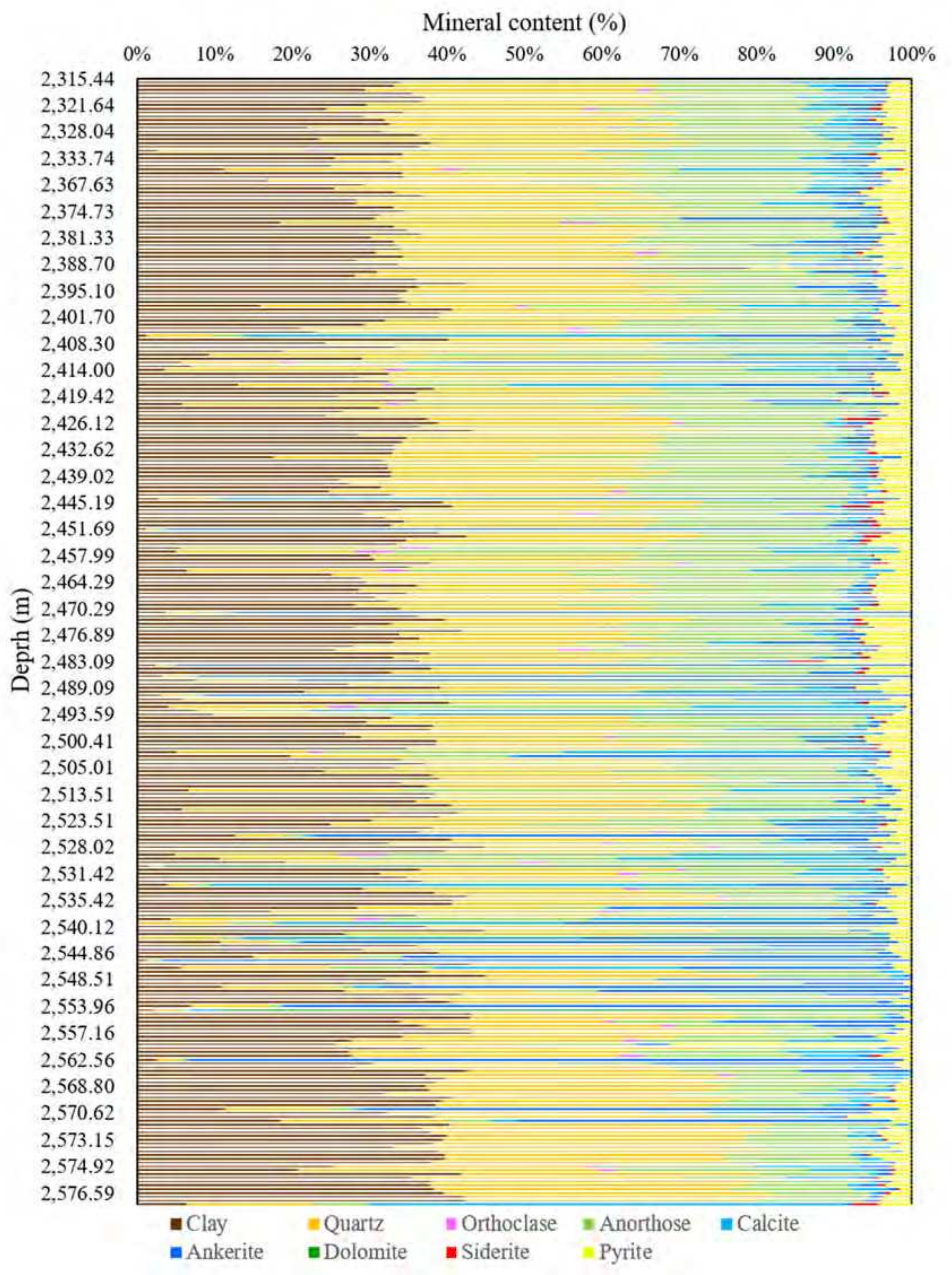

Figure 5. Results of XRD analyses showing the mineral composition of the shale oil reservoir.

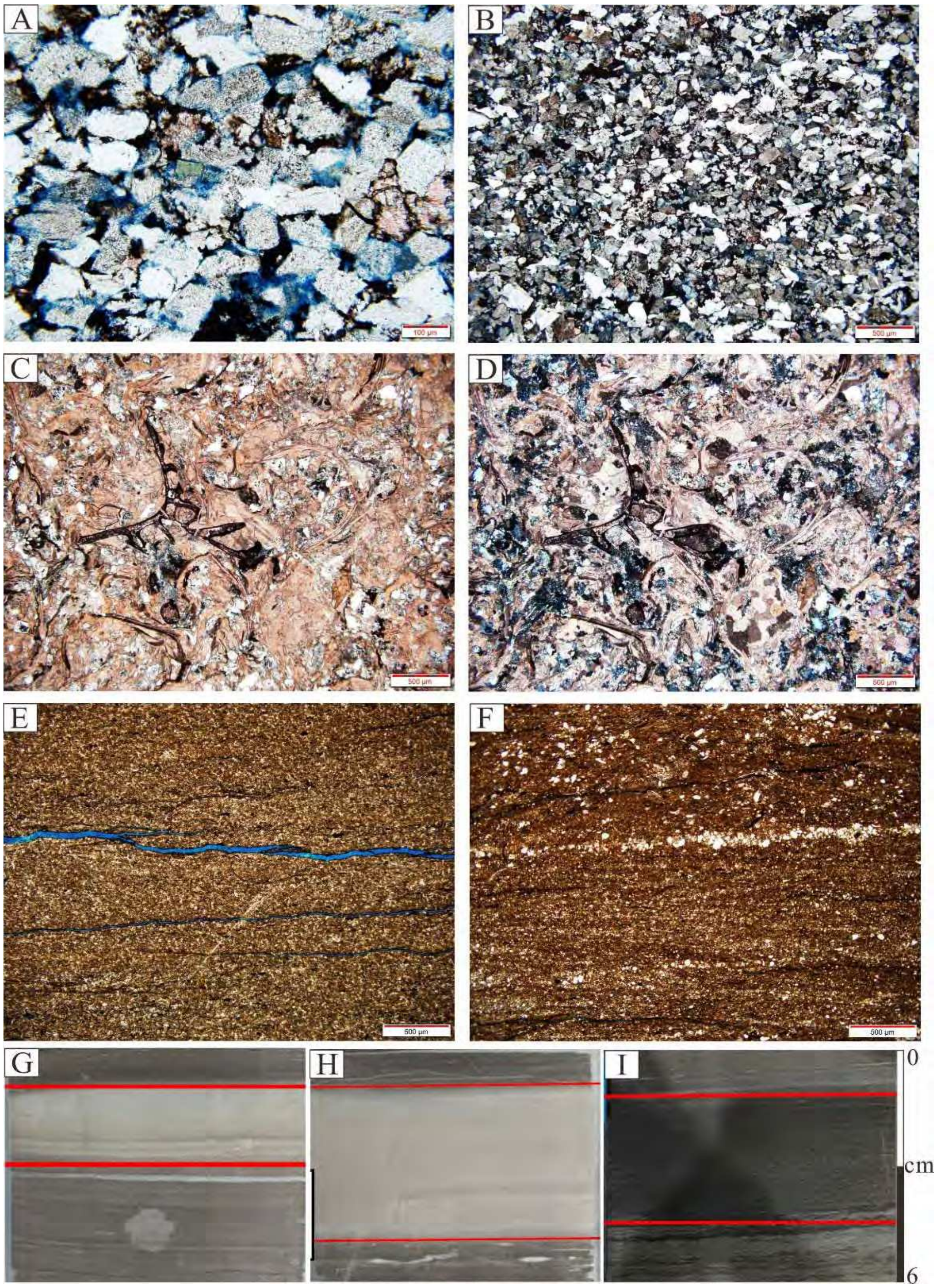

Figure 6. Thin sections and core photos showing examples of lithology in the Cretaceous Qingshankou Formation, Gulong Sag, Songliao Basin. A, B. Siltstone, Well A, 2374.88 m; C, D. Shell limestone, Well A, 2373.86 m; E, F. Shale, Well A, 2254.43 m; G. Dolostone, Well B, 2561.39 m; H. Dolostone, Well B, 2493.82 m; I. Mudstone, Well B, 2492.32 m.

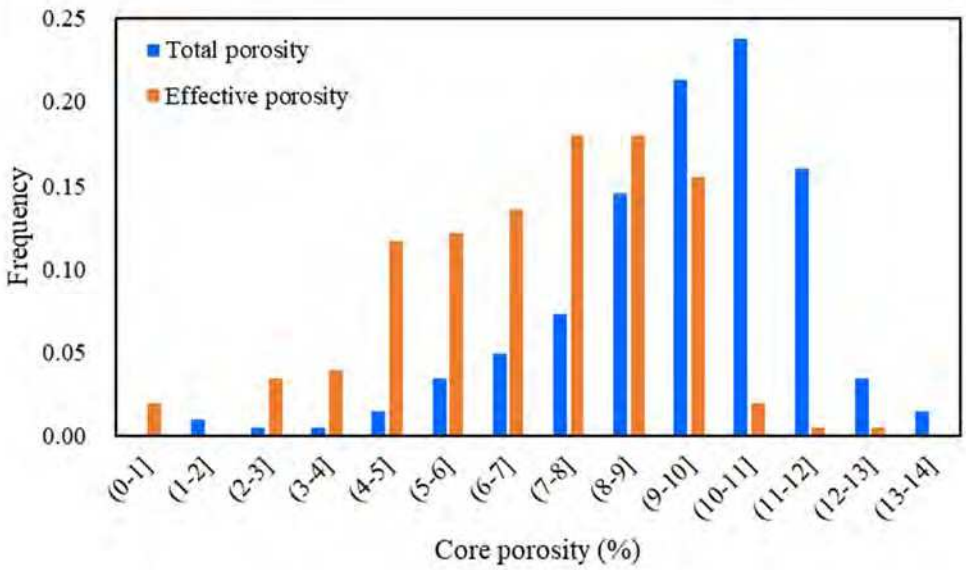

Figure 7. Frequency distribution of core porosity in the Qingshankou Formation, Gulong Sag, Songliao Basin (206 samples data of Well B).

Table 1. The classification standard of three types of lamina structure

Types of lamina structure	Laminated rocks	Layered rocks	Massive rocks
The thickness of each single layer (core observation)	Less than 0.01 m	Range from 0.01 m to 0.1 m	Larger than 0.1 m or no obvious layer
The density of layer (slab)	More than 100/m	Between 10/m and 100/m	No layers
Frequency of peaks and troughs (button conductivity curve)	More than 150/m	Between 20/m and 150/m	Less than 20/m

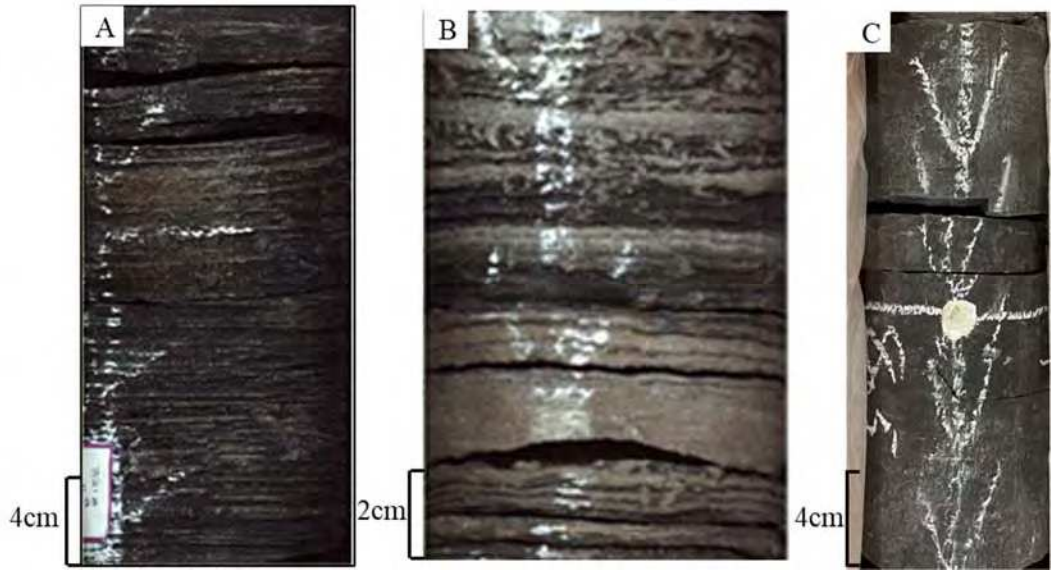

Figure 8. Core photos showing typical examples of lamina structure in the Cretaceous Qingshankou Formation, Gulong Sag, Songliao Basin. A. Laminated rocks in shale. B. Layered rocks in shale. C. Massive rocks in mudstone.

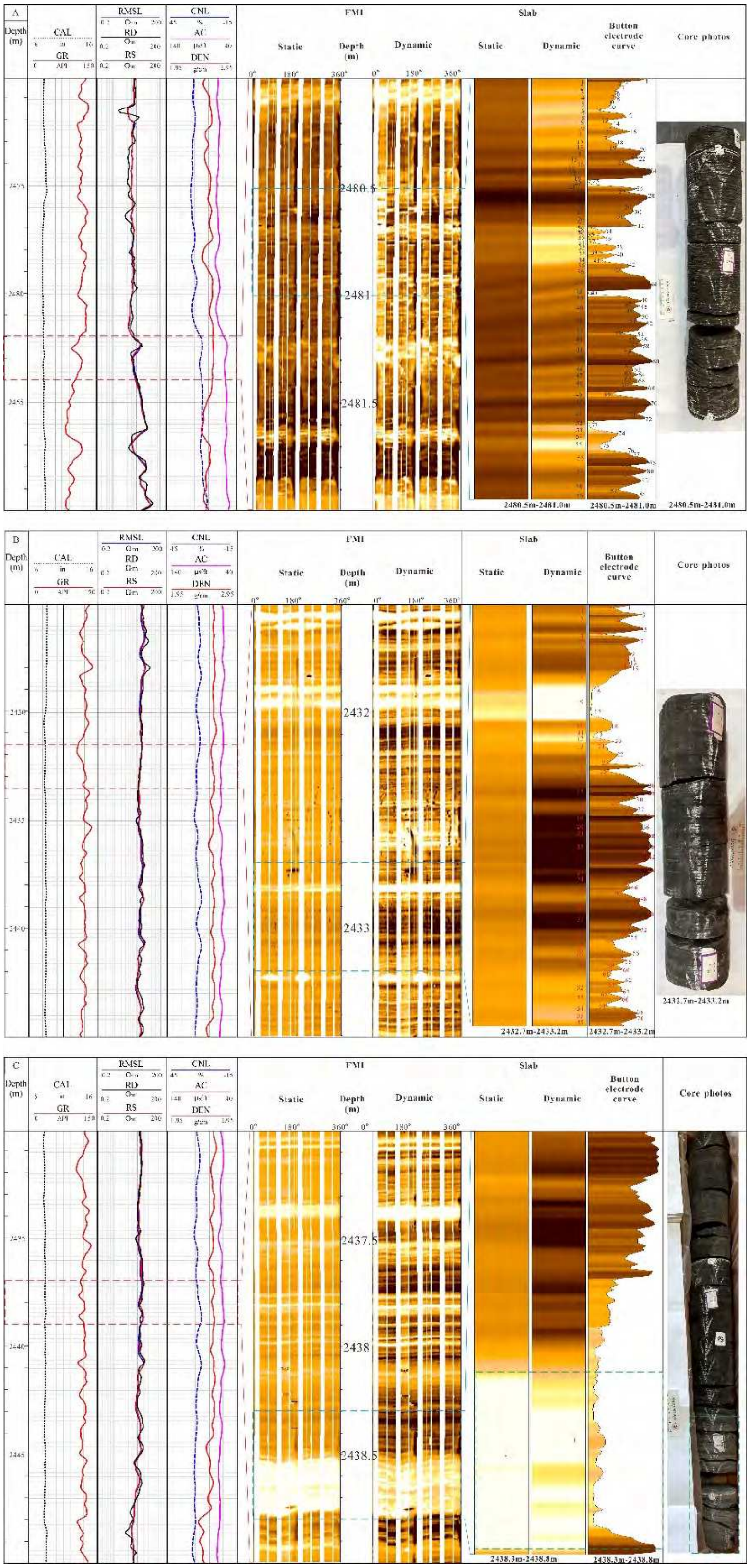

Figure 9. Well log response of three types of lamina structure in shale (well Y). A. Well log response of laminated rocks. B. Well log response of layered rocks. C. Well log response of massive rocks.

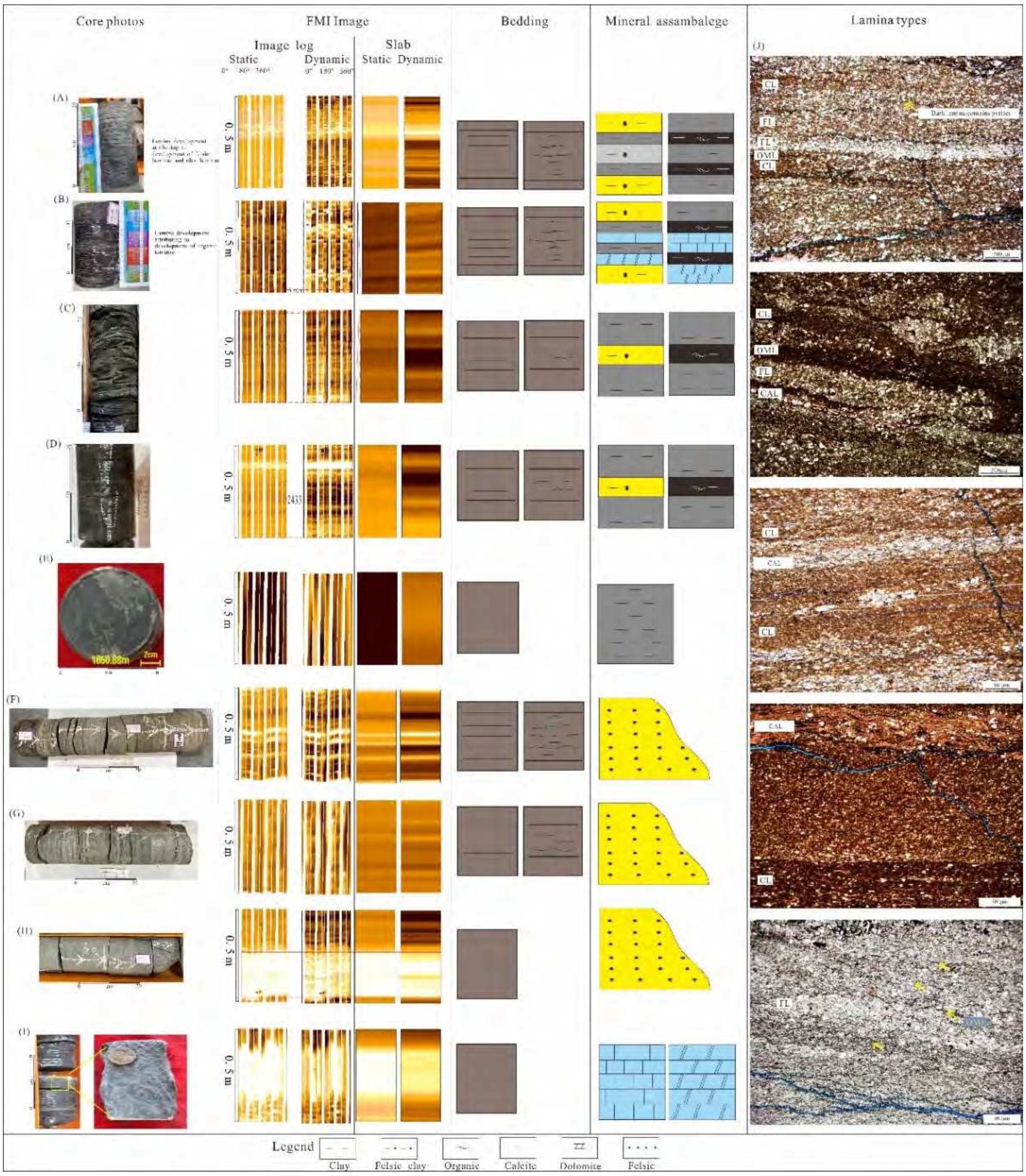

Figure 10. Lithology and lamina structure within shale of the Qingshankou Formation. Cores, wireline logs, thin sections, image logs, and button conductivity curves show examples of each lithology and their multi-scale lamina structure. Core photos, FMI images, slabs, and diagrams of lamina and mineral assemblages show example of each individual lithology. A. Laminated shale with felsic and clay laminae development. B. Laminated shale with organic and clay laminae development. C. Layered shale with bedding-parallel fractures developed. D. Layered shale. E. Massive mudstone. F. Laminated siltstone. G. Layered siltstones. H. Massive siltstone. I. Massive limestone. J. Various laminae types, including organic matter lamina (OML), felsic lamina (FL), clay lamina (CL), and carbonate lamina (CAL).

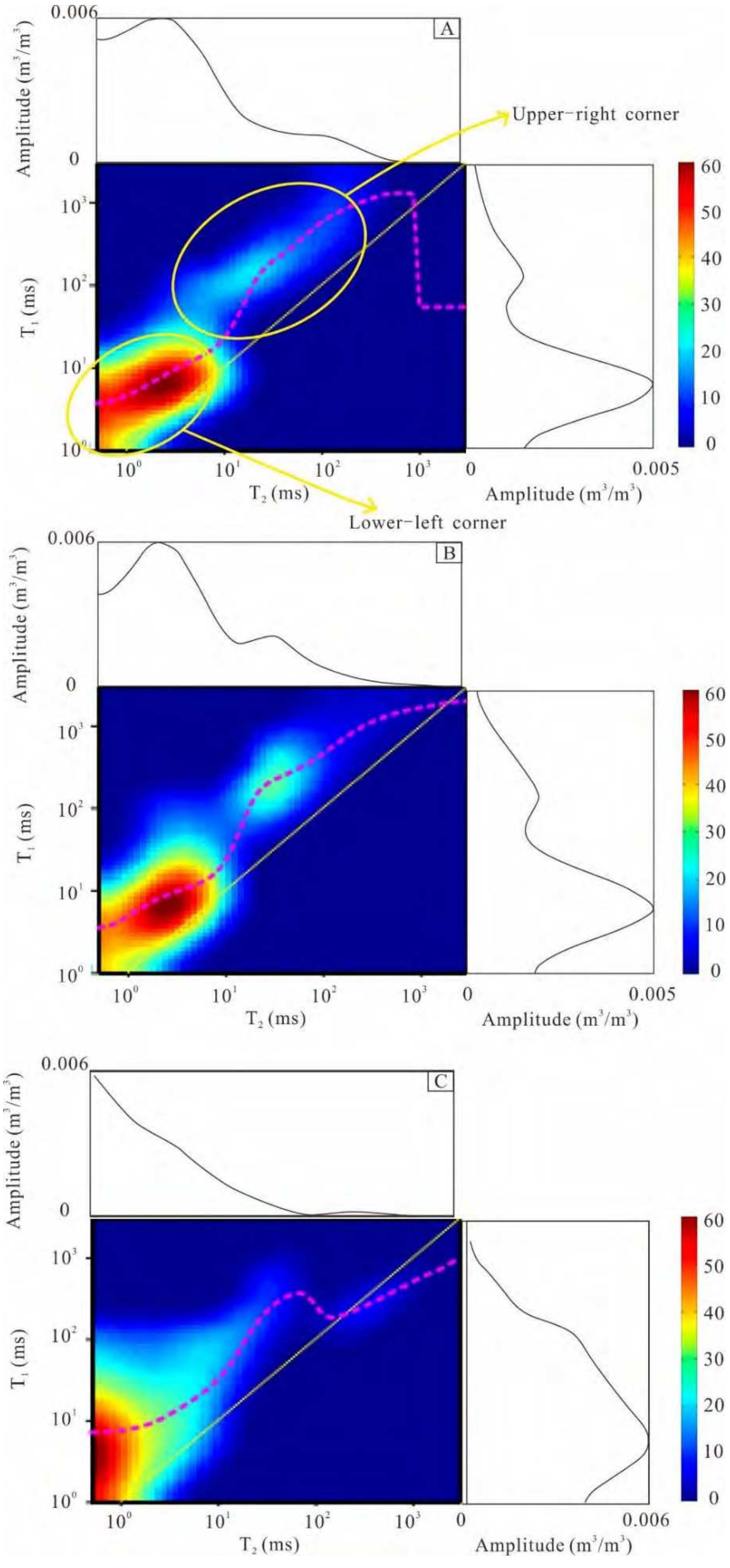

Figure 11. Three types T_1-T_2 map corresponding to the three types of lamina structure in the Cretaceous Qingshankou Formation, Gulong Sag, Songliao Basin.

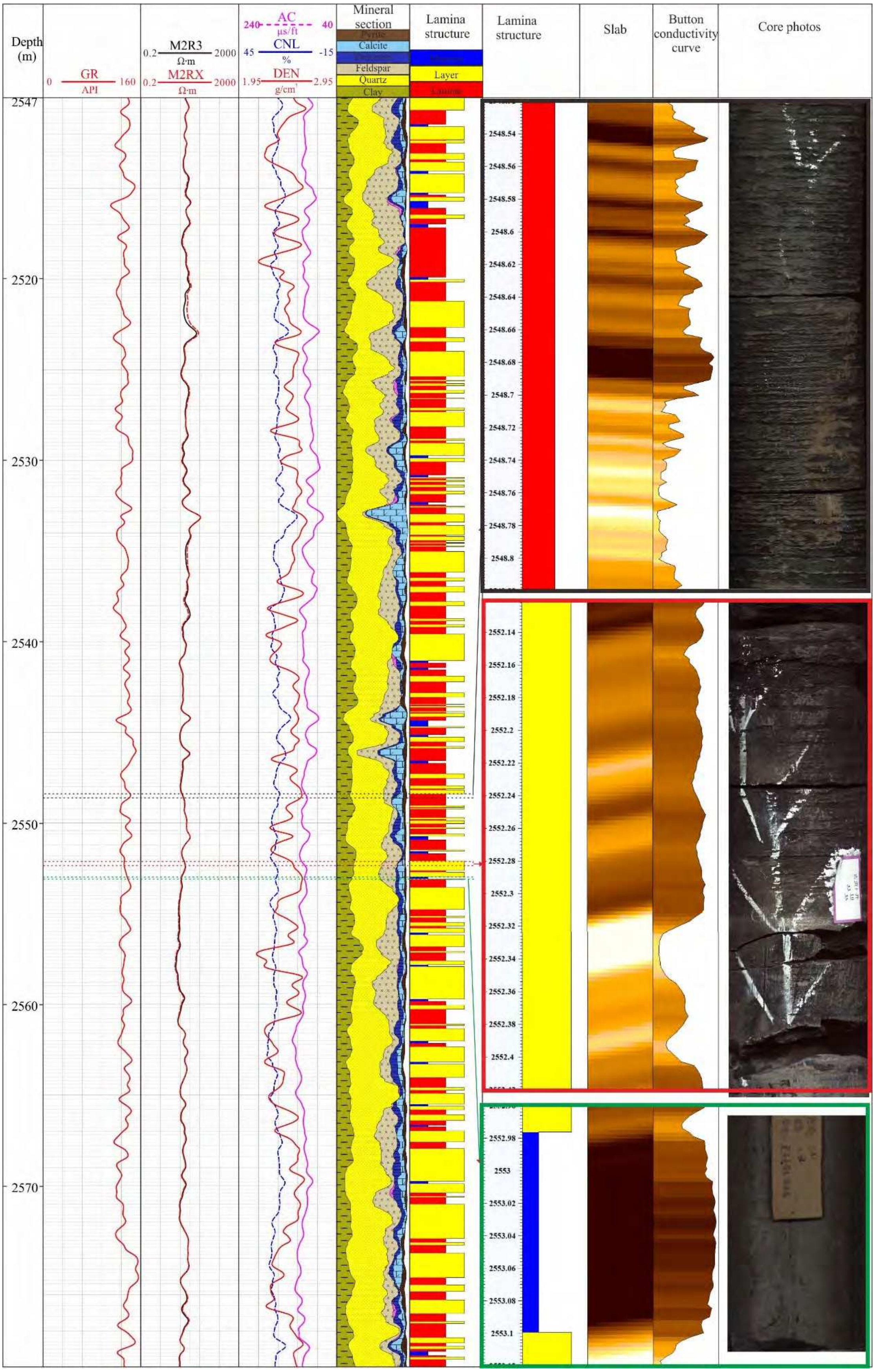

Figure 12. Lamina structure distribution in a single well in the Cretaceous Qingshankou Formation (well X). Tracks 7, 8, 9, and 10 are from strata at the same depth.

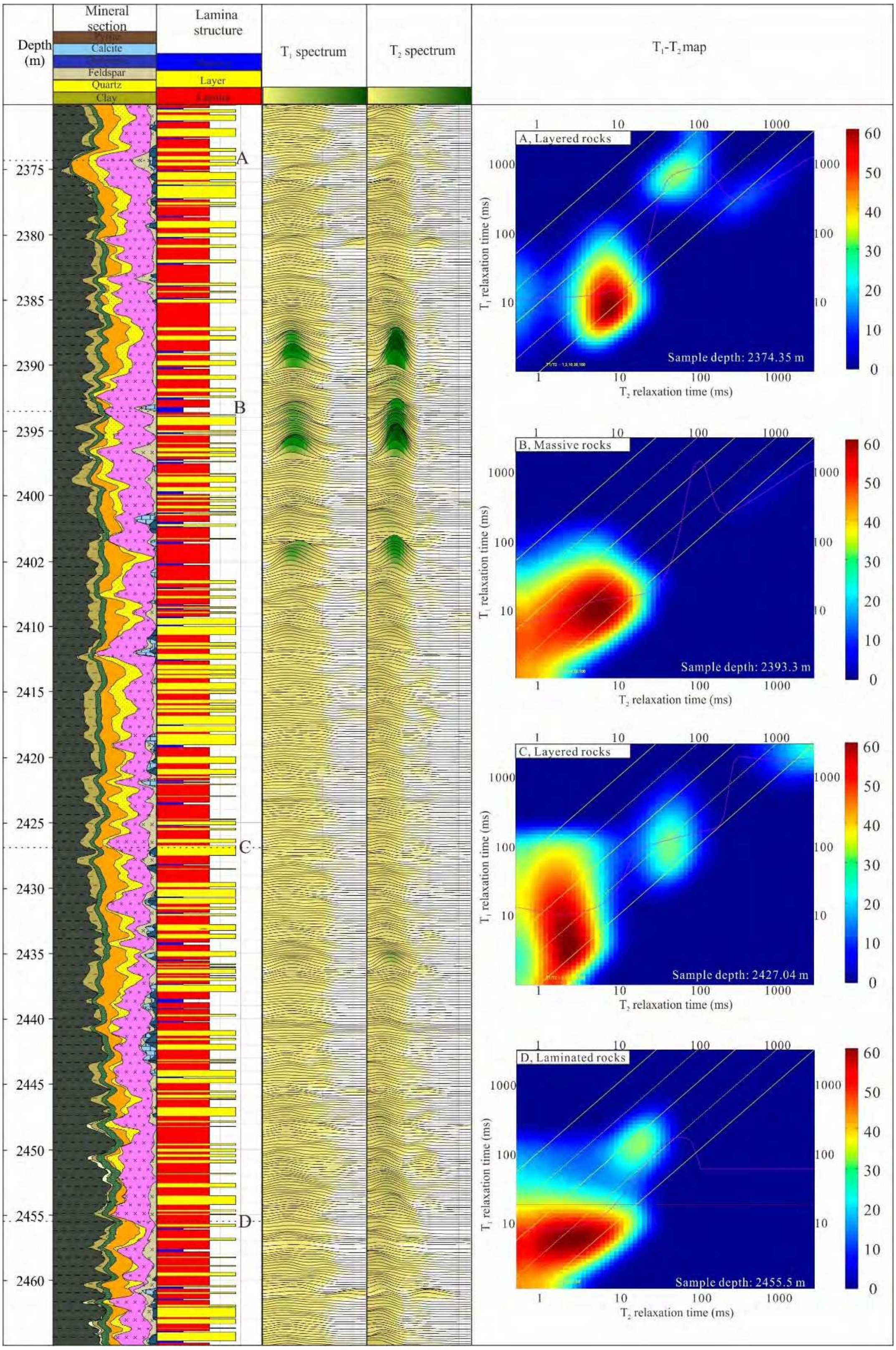

Figure 13. Relationships between lamina structure and reservoir quality and oil-bearing properties in shale in the Cretaceous Qingshankou Formation, Songliao Basin (well Y).

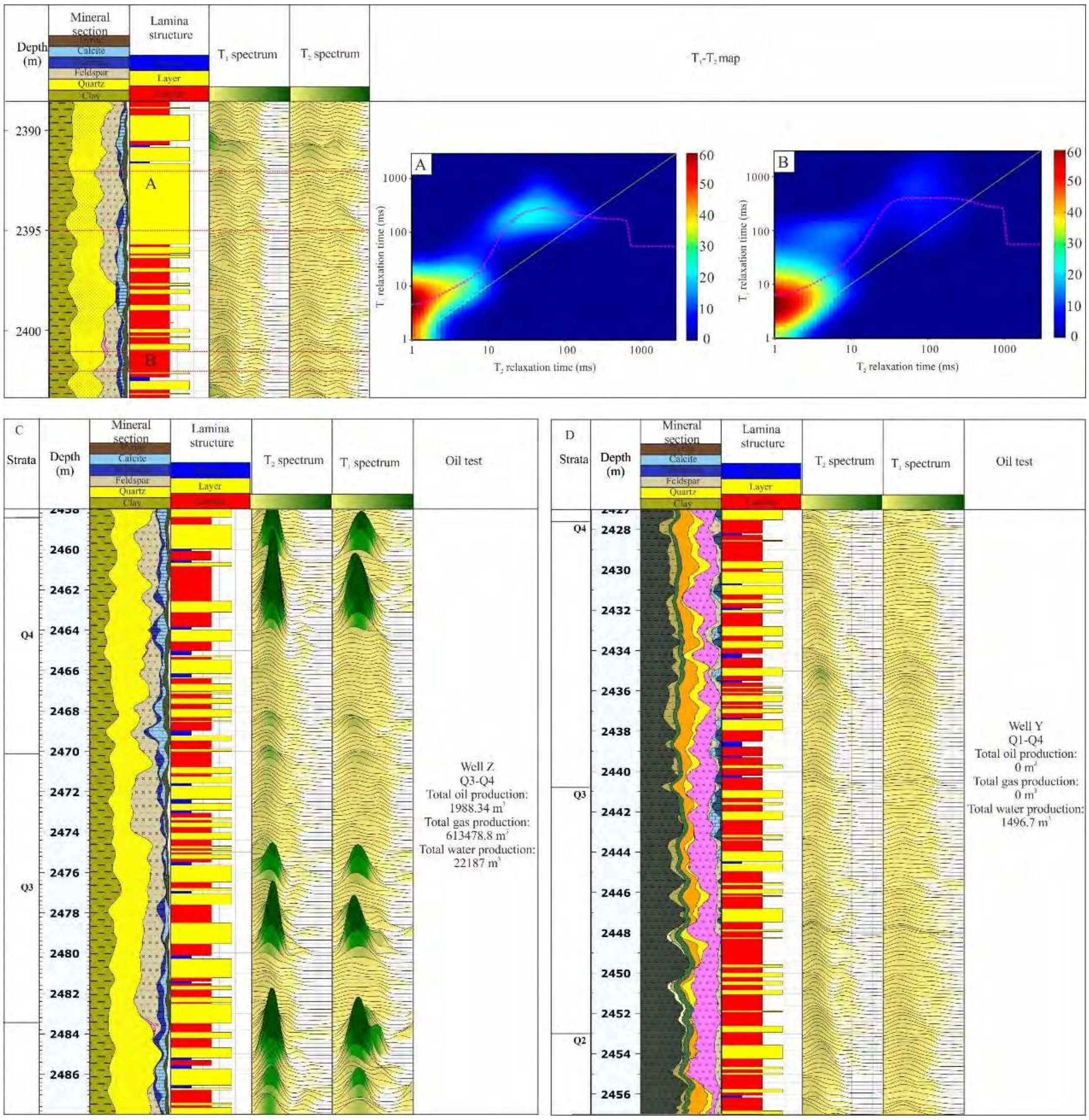

Figure 14. Relationships between laminae structure and reservoir quality and oil-bearing properties in shale in the Cretaceous Qingshankou Formation, Songliao Basin. Interval A (2392.0 m－2395.0 m) is layered rocks in well Z; interval B (2401.2 m－2402.0 m) is laminated rocks in well Z.

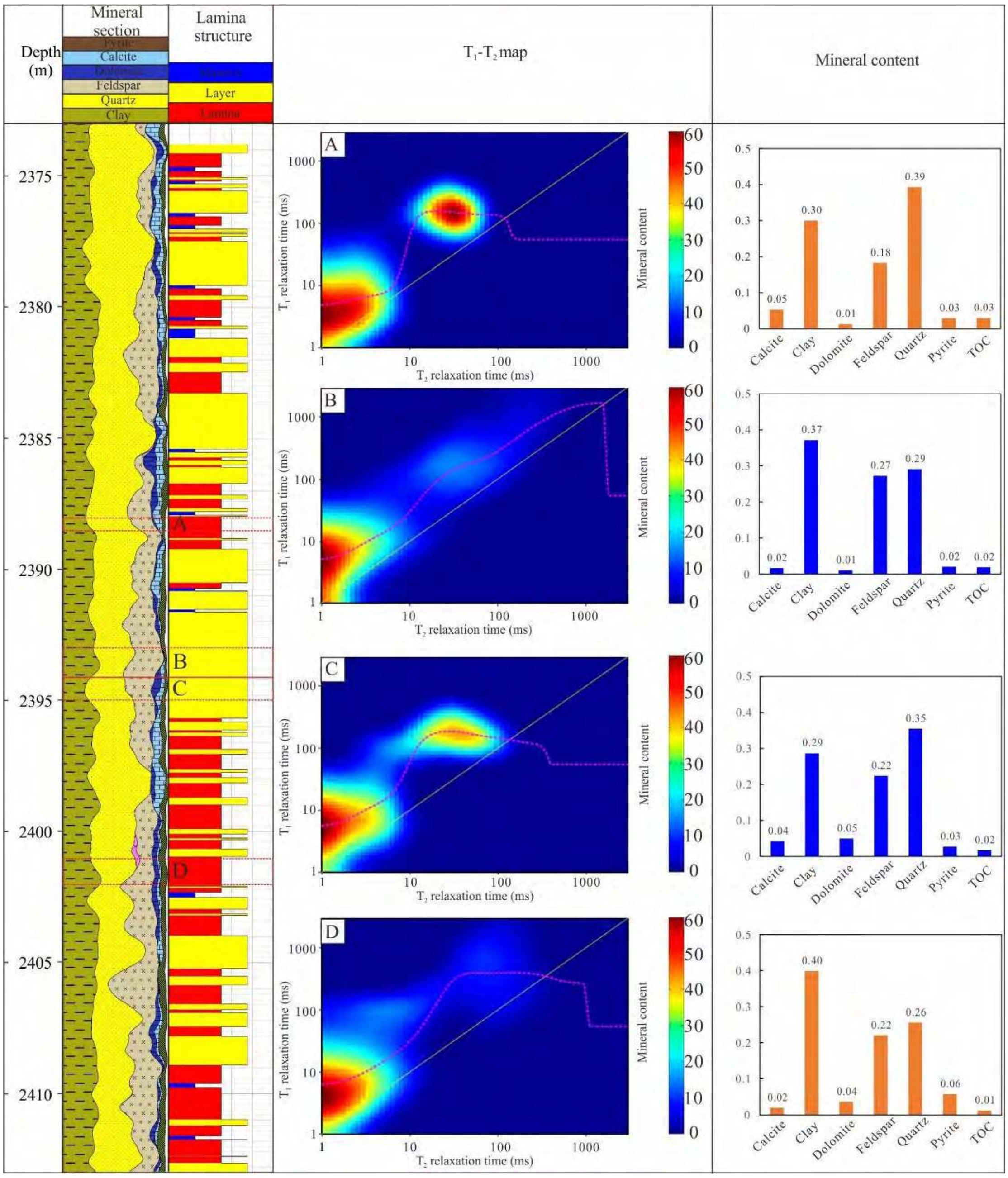

Figure 15. The effect of mineral content on the reservoir quality and oil-bearing properties in shale in the Cretaceous Qingshankou Formation, Songliao Basin (Well Z). A. laminated rocks. B. layered rocks. C. layered rocks. D. laminated rocks.